UCSF

Title

Anti-GD2 synergizes with CD47 blockade to mediate tumor eradication

Authors

Theruvath, Johanna
Menard, Marie
Smith, Benjamin AH
et al.

Anti-GD2 synergizes with CD47 blockade to mediate tumor eradication

Johanna Theruvath[1], Marie Menard[2,20], Benjamin A. H. Smith[3,4,20], Miles H. Linde[5,6,7,8,20], Garry L. Coles[1,7], Guillermo Nicolas Dalton[1], Wei Wu[9], Louise Kiru[9], Alberto Delaidelli[10], Elena Sotillo[7], John L. Silberstein[5,11], Anna C. Geraghty[12], Allison Banuelos[6,7], Molly Thomas Radosevich[1], Shaurya Dhingra[1], Sabine Heitzeneder[7], Aidan Tousley[1], John Lattin[1], Peng Xu[1], Jing Huang[1], Nicole Nasholm[2], Andy He[1], Tracy C. Kuo[13], Emma R. B. Sangalang[13], Jaume Pons[13], Amira Barkal[6,7,14,15], Rachel E. Brewer[6,7,14], Kristopher D. Marjon[6,7,14], Jose G. Vilches-Moure[16], Payton L. Marshall[15], Ricardo Fernandes[17,18], Michelle Monje[1,6,7,12,14,19], Jennifer R. Cochran[11], Poul H. Sorensen[10], Heike E. Daldrup-Link[1,6,9], Irving L. Weissman[6,7,14,19], Julien Sage[1,7], Ravindra Majeti[6,7,8,14], Carolyn R. Bertozzi[3,4], William A. Weiss[2], Crystal L. Mackall[1,7,8], Robbie G. Majzner[1,7,✉]

[1]Department of Pediatrics, Stanford University School of Medicine, Stanford, CA, USA.

[2]Departments of Neurology, Pediatrics, and Neurological Surgery, Brain Tumor Research Center, University of California, San Francisco, San Francisco, CA, USA.

³ChEM-H Institute, Stanford University, Stanford, CA, USA.

⁴Department of Chemical & Systems Biology, Stanford University, Stanford, CA, USA.

⁵Immunology Graduate Program, Stanford University School of Medicine, Stanford, CA, USA.

⁶Institute for Stem Cell Biology and Regenerative Medicine, Stanford, CA, USA.

⁷Stanford Cancer Institute, Stanford University School of Medicine, Stanford, CA, USA.

⁸Department of Medicine, Stanford University School of Medicine, Stanford, CA, USA.

⁹Department of Radiology, Stanford University School of Medicine, Stanford, CA, USA.

¹⁰British Columbia Cancer Agency, Vancouver, BC, Canada.

¹¹Department of Bioengineering, Stanford University Schools of Engineering and Medicine, Stanford, CA, USA.

¹²Department of Neurology and Neurological Sciences, Stanford University, Stanford, CA, USA.

¹³ALX Oncology, Burlingame, CA, USA.

¹⁴Ludwig Center for Cancer Stem Cell Research and Medicine, Stanford University School of Medicine, Stanford, CA, USA.

¹⁵Stanford Medical Scientist Training Program, Stanford University, Stanford, CA, USA.

¹⁶Department of Comparative Medicine, Stanford University School of Medicine, Stanford, CA, USA.

¹⁷Chinese Academy of Medical Sciences (CAMS) Oxford Institute (COI), University of Oxford, Oxford, UK.

¹⁸Nuffield Department of Medicine, University of Oxford, Oxford, UK.

¹⁹Department of Pathology, Stanford University School of Medicine, Stanford, CA, USA.

²⁰These authors contributed equally: Marie Menard, Benjamin A. H. Smith, Miles H. Linde.

Abstract

The disialoganglioside GD2 is overexpressed on several solid tumors, and monoclonal antibodies targeting GD2 have substantially improved outcomes for children with high-risk neuroblastoma. However, approximately 40% of patients with neuroblastoma still relapse, and anti-GD2 has not mediated significant clinical activity in any other GD2⁺ malignancy. Macrophages are important mediators of anti-tumor immunity, but tumors resist macrophage phagocytosis through expression of the checkpoint molecule CD47, a so-called 'Don't eat me' signal. In this study, we establish potent synergy for the combination of anti-GD2 and anti-CD47 in syngeneic and xenograft mouse models of neuroblastoma, where the combination eradicates tumors, as well as osteosarcoma and small-cell lung cancer, where the combination significantly reduces tumor burden and extends survival. This synergy is driven by two GD2-specific factors that reorient the balance of macrophage activity. Ligation of GD2 on tumor cells (a) causes upregulation of surface calreticulin, a pro-phagocytic 'Eat me' signal that primes cells for removal and (b) interrupts the interaction of GD2 with its newly identified ligand, the inhibitory immunoreceptor Siglec-7. This

work credentials the combination of anti-GD2 and anti-CD47 for clinical translation and suggests that CD47 blockade will be most efficacious in combination with monoclonal antibodies that alter additional pro- and anti-phagocytic signals within the tumor microenvironment.

The disialoganglioside GD2 is consistently overexpressed in neuroblastoma[1] and osteosarcoma[2,3] and is variably expressed in other sarcomas[3], gliomas[4], neuroendocrine tumors[5] and epithelial cancers[6]. Anti-GD2 antibodies have improved survival rates for patients with neuroblastoma only when administered as part of intense chemotherapy-based cytotoxic regimens[7–9], which are associated with debilitating late effects, including hearing loss, growth retardation and secondary leukemias[10,11]. Despite the integration of anti-GD2 antibodies into upfront treatment protocols, at least 40% of patients with neuroblastoma still relapse[7,9], and most of them eventually die of their disease[12]. Additionally, despite broad expression of GD2 on osteosarcoma, anti-GD2 antibodies have not mediated significant anti-tumor activity in that disease or any other GD2+ cancer, including small-cell lung cancer (SCLC)[13–15]. The mechanisms of immune evasion from GD2-directed antibodies in neuroblastoma and other diseases remain largely undefined.

Macrophages play an important role in the anti-tumor immune response by phagocytosing cancer cells, a process that is driven by engagement of their Fc receptors by antibodies. Macrophage phagocytosis of tumor cells is governed by a balance of pro- and anti-phagocytic inputs, so-called 'Eat me' and 'Don't eat me' signals[16]. CD47 is a checkpoint molecule that is overexpressed on tumor cells and inhibits macrophage activity through interaction with its receptor SIRPα[17]. CD47 blockade has shown promising clinical activity in early human trials[18,19]. In particular, the combination of rituximab, a CD20-targeted antibody, with anti-CD47 is effective in inducing remissions in patients with otherwise rituximab-resistant lymphomas[19,20]. It is unclear which other tumor-targeted antibodies would effectively combine with CD47 blockade.

We investigated whether anti-CD47 enhances the efficacy of anti-GD2 in neuroblastoma and other GD2+ malignancies. We show substantial synergy of these two agents, resulting in the recruitment of tumor-associated macrophages (TAMs) to mediate robust and durable anti-tumor responses. The responses are driven by factors specific to GD2 that reorient the balance of macrophage activity toward phagocytosis of tumor cells, including disruption of a newly identified GD2:Siglec-7 axis. These results show the unique synergy of combining anti-GD2 with anti-CD47, which has the potential to significantly enhance outcomes for children with neuroblastoma and osteosarcoma.

Results

Potent synergy of anti-GD2 and anti-CD47.

We first studied the combination of anti-GD2 and anti-CD47 in neuroblastoma, the only cancer for which anti-GD2 has been clinically validated. We measured phagocytosis of GD2+ neuroblastoma cells by human macrophages in vitro using a flow-based phagocytosis assay after treatment with anti-GD2 (dinutuximab, chimeric mouse/human IgG1 antibody), anti-CD47 (B6H12, murine IgG1 antibody) or a combination of both antibodies. The

combination of anti-GD2 and anti-CD47 resulted in significantly increased of phagocytosis of neuroblastoma cells (Fig. 1a,b). We confirmed these findings using live cell imaging (Extended Data Fig. 1a–d). Concentrations of anti-GD2 and/or anti-CD47 antibodies between 1 μg ml^{-1} and 20 μg ml^{-1}, which are below typical plasma concentrations achieved in human studies[18,21], were similarly active in inducing phagocytosis (Extended Data Fig. 1e).

Using an aggressive in vivo para-orthotopic (engrafted into the kidney capsule) xenograft model of *MYCN*-amplified neuroblastoma (KCNR), neither anti-GD2 nor anti-CD47 mediated significant anti-tumor effect, but the combination resulted in complete tumor eradication and long-term survival (Fig. 1c–f). We also performed this experiment with the clinically validated humanized anti-CD47 antibody magrolimab (Hu5F9-G4, humanized IgG4 antibody)[19], which showed similarly profound anti-tumor activity when combined with anti-GD2 (Extended Data Fig. 2a,b).

To demonstrate the generalizability of our approach, we repeated this experimental setup with a *MYCN*-non-amplified (MYCN-NA) neuroblastoma cell line (CHLA255) in both metastatic (Fig. 1g–j) and para-orthotopic (Extended Data Fig. 2c–f) models. In both models, the combination of anti-GD2 and anti-CD47 mediated potent and synergistic anti-tumor activity, resulting in cure of dual-treated mice. Thus, the combination of anti-GD2 and anti-CD47 is highly synergistic in xenograft models of neuroblastoma and mediates tumor eradication even when the single agents are completely ineffective.

Synergy of anti-GD2 and anti-CD47 dependent on macrophages.

The immunocompromised NOD scid gamma (NSG) mice in our models lack lymphocytes involved in a coordinated anti-tumor immune response; it was, therefore, unclear how this therapeutic combination would perform in an immune competent model. Using allografts from the well-described TH-MYCN syngeneic neuroblastoma model[22], we investigated the addition of CD47 blockade to a murine anti-GD2 antibody (14G2a, murine IgG2a) (Fig. 2a). As the commercially available anti-murine CD47 antibodies are low affinity and minimally effective in vivo[23,24], we used a fusion of murine IgG1 to a mutated form of SIRPα capable of binding mCD47 with 3.41 nM affinity (ALX301; Extended Data Fig. 3a–c). The IgG1 component was engineered with an N297A mutation to minimize interaction with the murine Fc receptor, decreasing the potential for off-tumor toxicity. This molecule binds specifically to murine CD47 and is capable of blocking its interaction with SIRPα on murine macrophages.

As in the xenograft models, the addition of CD47 blockade to anti-GD2 substantially enhanced anti-tumor responses, resulting in long-term, tumor-free survival of all combination-treated mice in the syngeneic model (Fig. 2b,c). Myeloid cell depletion with clodronate and anti-CSF1R antibody ablated the anti-tumor efficacy (Fig. 2d,e), indicating that the response to anti-GD2/CD47 blocker is dependent on the myeloid compartment. To further delineate which myeloid cells were involved in our models, we used anti-murine Ly6G antibody to selectively deplete neutrophils and granulocytes in NSG mice (Fig. 2f) but observed no effect on the anti-tumor activity (Fig. 2g), indicating that monocytic cells are likely responsible for the synergistic responses to anti-GD2/anti-CD47.

Lack of on-target toxicity with anti-GD2/anti-CD47.

GD2 is identical in mice and humans and is expressed on normal neural tissues in both species[25–28]. Treatment with anti-GD2 antibodies is associated with a temporary painful neuropathy syndrome in patients[7], thought to be caused by the engagement of GD2 on peripheral nerves and potentially related to complement fixation and/or direct electrophysiologic effects on nerve fibers[29,30]. To test whether the addition of anti-CD47 potentiates off-tumor effects of anti-GD2, we evaluated mice for signs of neurotoxicity in response to treatment. Immunocompetent mice receiving anti-GD2 (14G2a), CD47 blockade (ALX301) or anti-GD2 and CD47 blockade did not show weight loss (Fig. 3a) or signs of pain or neurologic distress. To evaluate potential functional neurological effects of treatment, we tested motor behavioral performance using CatWalk gait analysis during treatment[31]. CatWalk gait analysis showed no differences between treatment groups in swing speed of the limbs, stride length during normal gait or regularity index, a parameter of inter-limb coordination of regular step sequences (Fig. 3b–e). Mice were then sacrificed for tissue analysis by a board-certified veterinary pathologist. There was no evidence of toxicity (as determined by bright-field microscopy) in any of the examined sections of cerebrum, cerebellum, peripheral nerve, heart, liver, kidney, spleen or lung (Fig. 3f). These experiments were repeated in tumor-bearing NSG mice with similar results (Extended Data Fig. 4). Thus, in our murine models, the combination of anti-GD2 and anti-CD47 does not cause neurologic or other toxicity that could preclude translation to human studies.

GD2-specific factors drive synergy of anti-GD2 and anti-CD47.

Having shown significant synergy of anti-GD2 and anti-CD47, we wondered whether CD47 blockade would similarly enhance the activity of other tumor-specific antibodies. We evaluated the combination of anti-CD47 with an anti-B7-H3 antibody (enoblituzumab, a humanized Fc enhanced IgG1 antibody[32]) both in vitro and in vivo. The addition of anti-B7-H3 to anti-CD47 was minimally effective in enhancing anti-tumor activity compared to anti-CD47 alone in either neuroblastoma or osteosarcoma xenografts (Extended Data Fig. 5). These results suggested that GD2-specific factors were responsible for the enhanced activity observed in our models, which we then set out to define.

Siglec-7 is the ligand for GD2.

We hypothesized that GD2 itself interacts with and inhibits immune cells in general and macrophages in particular. GD2 is a sialic acid linked glycolipid (a sialoglycan). Sialoglycans are known to be bound by Siglecs (sialic acid-binding immunoglobulin-like lectins), a family of receptors expressed on immune cells, including macrophages and natural killer (NK) cells, that generally suppress immune cell activity through their cytoplasmic immunoreceptor tyrosine-based inhibitory motif (ITIM) domains[33]. We screened recombinant versions of all commercially available human Siglecs for binding to the CHLA255 and KCNR neuroblastoma cell lines by flow cytometry and observed different degrees of binding with Siglec-5, Siglec-7, Siglec-9 and Siglec-14 (Fig. 4a).

Because tumor cells express many glycans capable of Siglec binding, we next sought to specifically assess whether GD2 binds any human Siglecs. To test this, we treated a GD2^{−} cell line (Nalm6) with a cocktail of sialidases to remove all sialic acids and, thus,

all Siglec ligands from the cell surface. We then incubated these sialidase-treated cells with commercially obtained GD2, whose hydrophobic tail was readily integrated into the cell membrane (Fig. 4b). We confirmed the presence of GD2 on the cell surface by flow cytometry (Fig. 4c) and then probed these GD2-coated cells with recombinant human Siglecs. We discovered that GD2 specifically binds to Siglec-7 and to no other human Siglecs (Fig. 4d). Additionally, lentiviral transfection of both *B4GALNT1* (GD2 synthase) and *ST8SIA1* (GD3 synthase) on Nalm6 to drive GD2 expression resulted in a substantial increase in Siglec-7 binding (Fig. 4e).

Siglec-7 is expressed on human macrophages and NK cells, consistent with the immune infiltrate common in neuroblastoma[34,35], and is capable of suppressing immune cell activity through its cytoplasmic ITIM domain[36,37]. Siglec-7:GD2 binding on Nalm6 cells artificially coated with GD2 was also interrupted by blocking with an anti-GD2 antibody (Fig. 4f). Additionally, we found robust binding of Siglec-7 to neuroblastoma cell lines that was specifically disrupted by anti-GD2 antibody (Fig. 4g), demonstrating that anti-GD2 antibodies are capable of blocking binding to Siglec-7, potentially preventing its suppressive effects on the immune system.

Anti-GD2 primes cancer cells for removal by macrophages.

It was previously reported that GD2 ligation can directly result in cell death of neuroblastoma cells in the absence of immune effectors[38,39]. We confirmed these findings with two neuroblastoma cell lines, showing that tumor cells were killed in response to GD2 ligation in vitro (Fig. 5a and Extended Data Fig. 6a,b). Additionally, anti-GD2 treatment increased levels of surface calreticulin (Fig. 5b,c, and Extended Data Fig. 6c), a pro-phagocytic 'Eat me' signal that is shuttled to the surface from the endoplasmic reticulum in response to cell stress[16,40]. Therefore, GD2 ligation by anti-GD2 antibody primes cells for removal by the immune system.

Taken together, the ability of anti-GD2 to disrupt GD2:Siglec-7 interactions and drive upregulation of calreticulin helps explain the synergy of anti-GD2 and anti-CD47. We propose a model wherein blocking GD2 binding to Siglec-7 removes an inhibitory 'Don't eat me' signal from the tumor to the macrophages, whereas GD2 ligation results in upregulation of calreticulin, an 'Eat me' signal on the tumor cell surface. In the presence of anti-CD47, the balance of macrophage activity is shifted toward phagocytosis, resulting in potent anti-tumor activity (Fig. 5d).

To demonstrate the functional consequences of GD2 blocking and ligation, we generated an Fc-dead version of dinutuximab[41]. This antibody is capable of binding GD2 on tumor cells (Fig. 5e) but does not bind human Fc receptor (Fig. 5f) or fix complement. Despite its inability to directly interact with macrophages, the antibody significantly synergized with anti-CD47 antibody in vivo, showing similar activity to the Fc-live version of the antibody when combined with CD47 blockade (Fig. 5g,h). Thus, rather than simply providing an activating Fc domain to macrophages, treatment with anti-GD2 antibody significantly tilts the balance of macrophage activity toward phagocytosis, resulting in enhanced anti-tumor activity when combined with CD47 blockade.

Anti-GD2/anti-CD47 is active in other GD2^{+} malignancies.

GD2 is also expressed on other malignancies, including the pediatric bone tumor osteosarcoma[2,3,42]. Almost all patients with osteosarcoma receive the same chemotherapy regimens as 30 years ago, which are associated with the highest frequency of late effects of any pediatric cancer[43], and patients with metastases or relapse suffer extremely poor outcomes[44]. Unfortunately, anti-GD2 antibody has not mediated significant clinical benefit for patients with osteosarcoma[13]. Many osteosarcoma tumors are infiltrated by macrophages[45], so we hypothesized that the addition of anti-CD47 would license these TAMs for anti-tumor activity in the setting of anti-GD2.

We confirmed that the combination of anti-GD2 and anti-CD47 was effective in vitro using phagocytosis assays with osteosarcoma cell lines (Fig. 6a). In an orthotopic xenograft model of osteosarcoma (MG63.3) (Fig. 6b), we observed no effect of either single antibody treatment but synergistic activity of the combination of anti-GD2 and anti-CD47 with significantly delayed tumor growth (Fig. 6c) and prolonged survival (Fig. 6d).

Most mortality from osteosarcoma in children is driven by lung metastases, which are present but undetectable at the time of initial tumor diagnosis and treatment[44]. In a recent clinical trial of children and young adults with relapsed osteosarcoma who were rendered free of disease by surgery, adjuvant treatment with dinutuximab (anti-GD2 antibody) and granulocyte-macrophage colony-stimulating factor did not prevent further relapses[13]. Drawing on a model of pulmonary metastatic osteosarcoma, we treated mice after amputation with a control antibody, anti-GD2, anti-CD47 or a combination of anti-GD2 and anti-CD47 (Fig. 6e). Anti-GD2 treatment alone did not alter the number or size of metastases, in line with findings from a recent clinical trial[13]. Although single-agent anti-CD47 reduced the number and size of metastases, only the combination of anti-GD2 and anti-CD47 eradicated nearly all metastases (Fig. 6f–h). Therefore, this approach might represent an approach to prevent pulmonary relapse in osteosarcoma, which is an area of pressing clinical need.

GD2 is also expressed on SCLC[5,46], an adult malignancy with especially poor outcomes despite adoption of immunotherapy into frontline regimens[47]. A recent randomized trial of chemotherapy with or without dinutuximab failed to show any advantage to treatment with anti-GD2 antibody in patients with SCLC[14]. To evaluate whether anti-GD2/anti-CD47 was active in another GD2^{+} malignancy, we tested the combination in a xenograft model of SCLC and observed significantly enhanced anti-tumor activity and survival (Extended Data Fig. 7a,b). Therefore, combination with anti-CD47 might expand the clinical use of GD2-targeting antibodies to other GD2^{+} diseases beyond neuroblastoma.

Anti-GD2/anti-CD47 recruits TAMs into an anti-tumor response.

We then evaluated tumors from mice implanted with orthotopic osteosarcomas that were treated with anti-GD2, anti-CD47 or the combination of both antibodies. Combination treatment was associated with an increase in macrophage infiltration and expression of inducible nitric oxide synthase (iNOS), consistent with the recruitment of TAMs to mediate anti-tumor activity usually associated with M1 macrophages (Fig. 6i–l). In

parallel, by flow cytometry, we observed a decreased percentage of immunosuppressive, M2 macrophages (Fig. 6m and Extended Data Fig. 8a). We also evaluated immune infiltrates in a neuroblastoma model and similarly observed increased macrophage numbers in anti-GD2/anti-CD47-treated mice (Extended Data Fig. 8b,c) with trends toward enhanced expression of iNOS (Extended Data Fig. 8d) and a reduction in TAMs with an M2 phenotype (Extended Data Fig. 8e,f).

We previously showed that tumor macrophage infiltration can be measured by magnetic resonance imaging (MRI) after intravenous administration of ferumoxytol nanoparticles that are selectively phagocytosed by macrophages[48]. We imaged a cohort of control and anti-GD2/anti-CD47-treated mice with osteosarcoma xenografts by MRI at 12 h after intravenous administration of ferumoxytol. Compared to control mice, we observed significantly reduced T2* relaxation values in combination-treated mice, indicative of increased ferumoxytol retention in the tumor tissue and consistent with enhanced macrophage infiltration, validating this approach for use as a potential biomarker in patients that would not require surgical biopsies, which is often not feasible in pediatric clinical trials (Fig. 6n–o).

GD2 levels may influence response to anti-GD2/anti-CD47.

To better understand which patients with neuroblastoma might best respond to CD47 blockade, we analyzed publicly available databases for a relationship between several biologically prognostic features in neuroblastoma (*MYCN* amplification, ploidy and age) and *CD47* mRNA expression. Across three datasets, *CD47* expression was higher in patients with MYCN-NA tumors but did not consistently correlate with either ploidy or age (Extended Data Fig. 9a). Interestingly, MYCN-NA tumors also showed higher expression of markers of macrophage infiltration, including *CD163*, *CD86* and *SIGLEC7* (Extended Data Fig. 9b). Thus, MYCN-NA neuroblastoma tumors are likely infiltrated by greater numbers of macrophages and might be more likely to respond to anti-GD2/anti-CD47. *CD47* expression, on the other hand, did not correspond to *MYC* expression in either osteosarcoma or SCLC (Extended Data Fig. 9c,d).

Although combination with anti-CD47 established the efficacy of anti-GD2 in osteosarcoma and SCLC xenografts, it was more efficacious in neuroblastoma models, on which GD2 density is significantly higher by flow cytometry (Extended Data Fig. 9e). GD2 expression in tumors can be heterogeneous, especially on sarcomas[3,49]. To better understand which patients might benefit most from the combination of anti-GD2 and anti-CD47, we asked whether expression levels of GD2 influence its anti-tumor activity. Drawing on isogenic cultures of a neuroblastoma cell line (SH-SY5Y) that expresses high versus low levels of GD2 (Extended Data Fig. 9f), we found that the activity of anti-GD2/anti-CD47 was significantly reduced when GD2 was expressed at lower levels (Extended Data Fig. 9g), indicating that GD2 density might be a predictor of response, a result that needs to be studied prospectively in human trials.

Discussion

In this study, we show synergy of anti-GD2 and anti-CD47 antibodies in seven separate murine models in multiple histologies, offering a potential approach to treat GD2+

malignancies. This combination will now be tested in a first-in-human/first-in-child clinical trial (NCT04751383) for children and young adults with neuroblastoma and osteosarcoma. If our results are validated in the clinic, this approach will provide a unique option for the treatment of GD2^{+} malignancies that could eventually reduce the reliance on highly cytotoxic chemotherapy. It is important to note that GD2 is also expressed on peripheral nerves, and any enhancement of immune activity against GD2^{+} tumor cells could also result in worsening of on-target, off-tumor toxicity. Although we did not observe any signs of neurotoxicity in our murine models, GD2 antibody-associated allodynia is not recapitulated in mice and requires specialized rat models for assessment[50]. Potential exacerbation of anti-GD2 antibody-mediated pain or other neurotoxicity needs to be carefully considered and monitored in any clinical trial.

Neuroblastoma tumors are often infiltrated by NK cells[34], which can mediate anti-tumor activity, but they are also highly infiltrated by macrophages[35], which are thought to play an immune suppressive role[51]. We show that anti-GD2/anti-CD47 recruits these TAMs into the anti-tumor response, rendering them capable of mediating complete tumor clearance. Unlike neuroblastoma, osteosarcomas and SCLCs are rarely infiltrated by NK cells[52,53], and the use of anti-GD2/anti-CD47 appears to elicit an immune response where anti-GD2 antibody alone is ineffective by unleashing the macrophage compartment. We observed synergistic effects of anti-GD2 and anti-CD47 in both NSG (lacking all functional T, B and NK cells) and 129X1/SvJ (immunocompetent but with some myeloid cell dysfunction[54]) mouse models. It is possible that responses will be more robust in patients with intact immune systems, including NK cells and macrophages, although patients who have been previously treated with cytotoxic chemotherapy may have compromised immune function.

The significant anti-tumor activity in our models derives from two GD2-specific factors. First, GD2 ligation directly results in tumor cell death and upregulation of surface calreticulin on tumor cells, driving macrophage phagocytosis. Like dinutuximab, the anti-CD20 antibody rituximab is known to drive direct tumor cell killing in lymphoma[20,55], and this might similarly account for the enhanced activity observed in human trials when combined with CD47 blockade[19]. Cytotoxic agents such as chemotherapy and radiation also increase surface expression of calreticulin on tumor cells and similarly enhance the efficacy of anti-CD47 in preclinical models[56].

Second, we identified the ligand for GD2 to be Siglec-7, an inhibitory receptor expressed by NK cells and macrophages. Anti-GD2 antibodies block the interaction of GD2 with Siglec-7 and therapeutically disrupt its inhibitory effects on the immune system. Similarly, the glycoprotein CD24 expressed on tumor cells was recently shown to bind Siglec-10 on macrophages and inhibit phagocytosis[57]. These data indicate an important role for Siglec molecules in governing phagocytosis and anti-tumor immunity based on the surface glycome of tumor cells. Blocking Siglec binding to glycolipids and glycopeptides is an emerging field of interest[58], and agents that target Siglec molecules have shown early activity in the clinic[59].

Using an Fc-dead version of dinutuximab, we showed that anti-GD2 mediates significant synergy with anti-CD47 independent of macrophage Fc receptors. We are unable to separate

the effects of GD2 ligation-driven calreticulin overexpression from interruption of GD2–Siglec-7 interactions because they both occur with antibody treatment. Generating GD2+ versus GD2− cell lines that are otherwise identical is not possible because knockout of a sialyltransferase or a glycosyltransferase in the ganglioside synthesis pathway results in upregulation of other precursor sialoglycans on the cell surface that might bind Siglec-7 or other Siglecs. Further studies will explore knockout of Siglecs in primary human monocytes and macrophages. Although combinations of anti-CD47 with some tumor-specific antibodies, such as anti-CD20, have been highly successful[19], others, such as anti-EGFR, have not been as promising[60]. Our findings provide important insights on the characteristics of tumor-specific antibodies that can provide synergy with anti-CD47 and result in anti-tumor activity in the clinic.

We also found that GD2 expression levels (antigen density) determine response to anti-GD2/anti-CD47. GD2 expression cannot be directly inferred from transcriptomic data because it is regulated by a network of multiple sialyltransferases and glycosyltransferases. Mechanisms of GD2 regulation in neuroblastoma and other cancers are poorly understood and are the subject of ongoing studies, which might help identify those patients who are most likely to respond to this and other anti-GD2-based immunotherapies. Whether CD47 and GD2 expression determine response to anti-GD2/anti-CD47 in patients will be studied in correlative studies as part of our clinical trial.

In conclusion, we showed significant synergy of anti-GD2 and anti-CD47 antibodies, credentialing this approach for a first-in-human/first-in-child clinical trial. Additionally, this work lays a framework for defining which types of tumor-specific antibodies are best combined with CD47 blockade, namely those capable of further enhancing phagocytosis by blocking other 'Don't eat me' signals and/or increasing expression of 'Eat me' signals. This mechanistically driven combination of anti-GD2/anti-CD47 has the potential to extend the benefits of anti-GD2 antibodies to additional patients with neuroblastoma and to reach patients with osteosarcoma and other GD2+ malignancies.

Online content

Any methods, additional references, Nature Research reporting summaries, source data, extended data, supplementary information, acknowledgements, peer review information; details of author contributions and competing interests; and statements of data and code availability are available at https://doi.org/10.1038/s41591-021-01625-x.

Methods

Cells and culture conditions.

Human cell lines used in these studies were supplied by the following sources: MG63.3 and 143b by C. Khanna (National Cancer Institute, National Institutes of Health), Nalm6 (American Type Culture Collection (ATCC)), KCNR and CHLA255 by R. Seeger (Keck School of Medicine, University of Southern California), SY5Y-GD2-hi by K. Stegmaier (Dana Farber Cancer Institute), SY5Y-GD2-low (ATCC) and NCI-H69 SCLC (ATCC). Some cell lines were stably transduced with green fluorescent protein (GFP) and firefly

luciferase using retrovirus as previously described[61]. GD2 knockout was achieved in KCNR and CHLA255 tumor cells using CRISPR–Cas9 to target the gene encoding GD2 synthase (*B4GALNT1*) and then sorted by fluorescence-activated cell sorting (FACS) as previously described for other cell lines[4]. Nalm6 was lentivirally transduced with vecors encoding *B4GALNT1* and *ST8SIA1* as previously described[62]. All tumor cell lines were cultured in RPMI-1640, supplemented with 10% heat-inactivated FBS (Gibco, Life Technologies), 10 mM HEPES, 100 U ml^{-1} of penicillin, 100 μg ml^{-1} of streptomycin and 2 mM L-glutamine (Gibco, Life technologies), referred to as cRPMI. Tumor cell line identity was regularly confirmed with STR fingerprinting, and cell lines tested negative for mycoplasma approximately every 6 months.

Flow cytometry.

Data were collected with an LSR Fortessa X-20 (BD Biosciences) or LSR II (BD Biosciences) using FACSDiva version 8.0.1 or a Cytek Aurora Cytometer (Cytek) using SpectroFlo version 2.2.0.4 and analyzed using FlowJo software version 10.8.0. Cells were harvested, washed with FACS buffer (PBS supplemented with 2% FBS) and stained for 30 min in the dark on ice. Cells were washed with FACS buffer after each incubation step. Representative gating strategies are shown in Supplemental Fig. 1. Antibodies used are shown in Supplementary Table 1.

Macrophage generation and stimulation.

Primary human-donor-derived macrophages were generated as previously described[57]. In brief, leukocyte reduction system chambers from anonymous donors were obtained from the Stanford Blood Center. Peripheral monocytes were purified through successive density gradients using Ficoll (Sigma-Aldrich) and Percoll (GE Healthcare). Monocytes were then differentiated into macrophages by 7–9 d of culture in IMDM + 10% AB human serum (Life Technologies).

In vitro flow-based phagocytosis assay.

For all flow-based in vitro phagocytosis assays, tumor cells and human macrophages were co-cultured at a ratio of 2:1 in ultra-low-attachment 96-well U-bottom plates (Corning) in serum-free RPMI (Thermo Fisher Scientific). Tumor cells either virally expressed GFP or were labeled with CFSE (Invitrogen) by suspending cells in PBS (5 μM working solution) as per manufacturer instructions for 20 min at 37 °C protected from light and washed twice with 20 ml of FBS-containing media before co-culture. Anti-GD2 (dinutuximab, acquired from United Therapeutics) or anti-B7-H3 (enoblituzumab, acquired from MacroGenics) was added alone or in combination with anti-CD47 (clone B6H12, Bio X Cell) at a concentration of 10 μg ml^{-1} (or the concentration indicated in the figures). Tumor cells and antibodies were incubated for 30 min in a humidified 5% CO_2 incubator at 37 °C. Plates were washed two times; human macrophages were added to the plate; and plates were incubated for 1–2 h at 37 °C. Phagocytosis was stopped by washing with 4 °C PBS and centrifugation at 336*g* before the cells were stained with Live/Dead stain and anti-CD11b. Assays were analyzed by flow cytometry, and phagocytosis was measured as the number of CD11b$^+$ and CFSE/GFP$^+$ macrophages, quantified as a percentage of the total CD11b$^+$ macrophages and normalized to the control condition.

Live cell phagocytosis assay.

Human macrophages were plated at a density of 15,000 cells per well in a 96-well plate overnight. The day of the assay, target cells were washed once with PBS and then labeled by incubation with 0.5 μg ml^{-1} of pHrodo Red (Essen BioScience) for 1 h. Cells were washed twice with complete media before adding 50,000 target cells to each well of the 96-well plate. Where indicated, 10 μg ml^{-1} of anti-GD2, 10 μg ml^{-1} of anti-CD47 or the combination of 10 μg ml^{-1} of both antibodies was added. Cells were allowed to settle for 10 min at room temperature before live cell imaging on an IncuCyte S3 (Essen BioScience). Phagocytosis was quantified as the area under the curve (AUC) of the integrated red intensity between 0 h and 24 h. Normalized phagocytosis was computed as the (AUC of the sample) / (AUC of the control group).

Molecular cloning, protein expression and purification of murine anti-CD47 (ALX301).

CV1 is a high-affinity human SIRPα variant that has been reported to bind mouse CD47 with affinity of 30 nM compared to wild-type SIRPα, which does not bind mouse CD47 (ref. [63]). To design a version of CV1 with further improved binding to mouse CD47, structural models of mouse CD47 and a high-affinity SIRPα were built based on reported FD6 complex structure (Protein Data Bank: 4KJY). From the modeled structures, various amino acid residues were identified and predicted to be critical for binding to mouse CD47. These mutations were explored experimentally, and ALX301 was generated using site-directed mutagenesis (QuickChange Lightning, Stratagene) to introduce V6I, A27I, I31R, K53R, E54D, H56P, L66T and S98I to the SIRPα domain, which was then subcloned and fused to mouse IgG1 N297A via GeneArt Seamless Plus Cloning Assembly Kit (Invitrogen) according to the manufacturer's instructions. The construct was expressed in 5-L scale Expi293 cells (Invitrogen) in shake flasks. Expression cultures were grown for 5 d at 37 °C in 8% CO$_2$ while shaking at 125 r.p.m. Supernatants were harvested via centrifugation and sterile-filtered. The protein was affinity purified using an AKTA avant 150 (GE Healthcare), bound to MabSelect SuRe LX resin (GE Healthcare), washed with 1× PBS, eluted with 0.1 M citric acid pH 3.3, neutralized with 10% v/v 1 M sodium phosphate pH 8 and dialyzed into 1× PBS, followed by a gel filtration polishing step where the main peak was pooled and collected. Then, 2 μg each of non-reducing and reducing protein samples were loaded onto a 4–20% Tris-Glycine gel (Invitrogen, cat. no. XP04205), run for 27 min at 270 V and then stained with InstantBlue (ISB1L) per the manufacturer's protocol.

Surface plasmon resonance.

All kinetics were determined on a Proteon XPR36 instrument (Bio-Rad) at 25 C. The running buffer was PBS pH 7.4 supplemented with 0.01% Tween 20. ALX301 was coupled to one ligand channel of a GLC sensor chip using standard amine coupling chemistry. Mouse CD47, expressed and purified in-house, was injected as analyte in a five-membered, three-fold dilution series with 100 nM top concentration using the 'single-shot kinetics' method. The sixth analyte channel was used as a buffer blank. The flow rate was 100 μl min^{-1}; the association time was 1 min; and the dissociation time was 10 min. The data were double-referenced using interspots and the buffer blank before fitting to a 1:1 Langmuir binding model with the ProteOn Manager software (version 3.1.0.6).

Cloning, expression and purification of dinutuximab and dinutuximab LALA-PG.

The gWIZ vector with a BM40 signal peptide was used for protein expression. DNA encoding dinutuximab's human IgG1 heavy chain with and without the LALA-PG mutation[64], along with DNA encoding dinutuximab's light chain, were ordered from Integrated DNA Technologies. Heavy and light chains were individually cloned into AscI/BamHI digested gWIZ vector using Gibson assembly. Plasmids were transfected into Expi293F cells (Thermo Fisher Scientific) in a 1:1 ratio of heavy chain:light chain using ExpiFectamine according to the manufacturer's instructions. Five days after transfection, supernatant was harvested, adjusted to pH 8.0 and sterile-filtered. Dinutuximab and dinutuximab LALA-PG were then purified using recombinant Protein A-Sepharose 4B (Thermo Fisher Scientific) buffer exchanged into antibody buffer (20 mM L-histidine, 250 mM sucrose, 0.05% polysorbate 20 pH 6.0) using Pierce Slide-A-Lyzer G2 Dialysis Cassettes (Thermo Fisher Scientific) and concentrated using Amicon Centrifugal Filters (Millipore Sigma). To assess GD2 and Fc binding, cells were stained with dinutuximab or dinutuximab LALA-PG and then stained with either anti-human secondary antibody or Alexa Fluor 647-labeled recombinant human Fc gamma RI/CD64 (R&D Systems).

14G2a production.

Anti-GD2 monoclonal antibody (14G2a) was produced using a hybridoma gifted by P. Sondel (University of Wisconsin). Purified antibody was generated by Bio X Cell after 0.2-μm filtration and protein A purification. The lot of antibody tested negative for murine pathogens and had an endotoxin level of less than 2 EU mg^{-1}.

Exogenous ganglioside coating.

GD2 (Matreya) was stored as a 1 mM stock solution in PBS at −20 °C. Cells were washed once with FACS buffer, and the concentration was adjusted to 4×10^6 cells per milliliter. Where indicated, cells were treated with a sialidase cocktail, comprising 100 nM each of *Vibrio cholerae* sialidase, *Arthrobacter ureafaciens* sialidase and *Clostridium perfringens* sialidase, for 30 min at 37 °C. The sialidases were expressed and purified in-house as previously described[65]. Cells were washed once with FACS buffer and then twice with PBS to remove BSA, as the presence of any residual protein was found to decrease the efficiency of labeling. The cell concentration was adjusted to 4×10^6 cells per milliliter in PBS, and stock GD2 was added to the cell suspension to achieve a final concentration of 200 μM. The solution was mixed by pipetting and incubated for 30 min on ice and then washed twice in FACS buffer before subsequent analyses.

Siglec ligand detection.

Siglec ligands were quantified via flow cytometry. First, 4 μg ml^{-1} of each Siglec-Fc (R&D Systems) was pre-complexed with 8 μg ml^{-1} of AffiniPure donkey anti-human IgG Alexa Fluor 647 (Jackson ImmunoResearch) in FACS buffer (0.5% BSA in PBS) for 30 min on ice. Cells were washed once with FACS buffer and then resuspended at 4×10^6 cells per milliliter. Where indicated, GD2 was blocked by staining with 10 μg ml^{-1} of anti-GD2 antibody (clone 14G2a, BioLegend) for 30 min on ice. Cells were again washed in FACS buffer and resuspended in 100 μl of the pre-complexed staining solution at 4×10^6 cells

per milliliter and incubated for 30 min on ice. The cells were then washed twice with FACS buffer. Dead cells were labeled using SYTOX Blue (Thermo Fisher Scientific) before performing flow cytometry on an LSR II (BD Biosciences).

Cell death and calreticulin assessment by flow cytometry.

100,000 neuroblastoma tumor cells were plated in triplicate in a 96-well plate (Corning) and treated with 10 μg ml^{-1} of dinutuximab for indicated time points at 37 °C. Cells were washed twice before staining with anti-calreticulin or isotype antibody for 30 min on ice protected from light. Afterwards, cells were washed with FACS buffer and stained with DAPI. For calreticulin, MFI was calculated as the difference between the mean fluorescence intensity (MFI) in the PE channel of the calreticulin-stained sample and the MFI in the PE channel of an isotype-stained sample from the same experimental condition.

Mice.

All animal studies were carried out under protocols approved by the Stanford University and University of California, San Francisco Animal Care and Use Committees. Immunodeficient NSG (NOD.Cg-Prkdcscid Il2rgtm1Wjl/SzJ) or immunocompetent 129X1/SvJ mice were ordered from Jackson Laboratory or bred in-house. TH-MYCN mice were bred in-house as previously described[22]. Mice used for in vivo experiments were between 6 and 12 weeks old, and equal numbers of male and female mice were used in all experimental groups. Mice were housed under standard conditions in line with institutional requirements. Group sizes are indicated in each figure legend. No statistical methods were used to pre-determine sample sizes, but our sample sizes are similar to those reported in previous publications[61].

Neuroblastoma in vivo models.

CHLA255 or KCNR tumor cells expressing green fluorescent protein (GFP) and luciferase (Luc) were expanded under standard culture conditions (described above) and harvested with trypsin (Gibco, Thermo Fisher Scientific). For the para-orthotopic experiments, 1×10^6 KCNR-GFP-Luc or 1×10^6 CHLA255-GFP-Luc tumor cells were implanted into the renal capsule as previously descibed[66]. Tumor growth was followed by bioluminescence intensity (BLI) on an IVIS Spectrum In Vivo Imaging System (PerkinElmer) 4 min after 3 mg of D-luciferin (PerkinElmer) was injected intraperitoneally. BLI values were quantified with Living Image version 4.5 software (PerkinElmer). Four days after tumor implantation, mice were randomized based on BLI, and antibody treatment was initiated. Then, 400 μg of IgG control (Bio X Cell), 400 μg of anti-CD47 (clone B6.H12, Bio X Cell), 400 μg of magrolimab (Hu5F9-G4, Forty Seven/Gilead), 300 μg of anti-B7-H3 (enoblituzumab, MacroGenics), 300 μg of anti-GD2 (dinutuximab, United Therapeutics) or combination treatments were administered intraperitoneally every other day for three doses. For the metastatic model experiments, 1 million CHLA255-GFP-Luc tumor cells were injected into the tail vein, and randomization and antibody treatment was performed as in the orthotopic models. For the Fc-dead experiment, 400 μg of IgG control (Bio X Cell), 400 μg of anti-CD47 (clone B6.H12, Bio X Cell), 300 μg of Fc-dead anti-GD2 (dinutuximab LALA-PG) or 300 μg of Fc-active anti-GD2 (dinutuximab) (generated as described above) or combination treatments were administered intraperitoneally twice in 3 d. Mice received two doses compared to three doses of the other antibody experiments performed in that model because

of limited antibody availability. For the toxicity experiment, 1 million CHLA255 tumor cells were engrafted as described above under the metastatic model. Mice were treated with PBS, 400 μg of anti-CD47 (clone B6.H12, Bio X Cell), 300 μg of anti-GD2 (dinutuximab, United Therapeutics) or combination treatments intraperitoneally three times per week for a total of seven doses. Weight was assessed serially, and behavioral analysis was performed as described below. At the end of the experiment, mice were sent for necropsy to assess tissues by a board-certified veterinary pathologist (details described below).

Osteosarcoma in vivo models.

MG63.3 osteosarcoma cells were expanded under standard culture conditions (described above) and harvested with trypsin (Gibco, Thermo Fisher Scientific). For the orthotopic model, 1 million MG63.3 cells were injected periosteal to the tibia of NSG mice. Antibody treatment with 400 μg of IgG control (Bio X Cell), 400 μg of anti-CD47 (clone B6.H12, Bio X Cell), 300 μg of anti-B7-H3 (enoblituzumab, MacroGenics), 300 μg of anti-GD2 (dinutuximab, United Therapeutics) or combination treatments were administered intraperitoneally three times per week starting 7 d after tumor engraftment for 4 weeks. Tumor growth was measured with digital calipers 1–2 times a week, and tumor area was calculated by multiplying lengths of the major and minor axes. Mice were euthanized when tumors exceeded a size set by institutional protocol.

For the metastatic model, orthotopic tumors were implanted as described above and allowed to grow for 30 d. The tumor-bearing leg of all mice was amputated using sterile technique under isoflurane anesthesia. Buprenorphine 0.05 mg kg^{-1} was injected subcutaneously for pain control. Mice were randomized to the treatment groups described above, based on their pre-amputation tumor sizes (groups were statistically identical). Antibody treatment was provided for a total course of 4 weeks. Thirty days after amputation, experimental mice were euthanized, and lungs were removed for evaluation of metastases. Lung metastases were quantified by counting the number of visible GFP$^+$ lesions on an ultraviolet gel box. Tissues were then formalin-fixed and further analyzed by immunohistochemistry (IHC).

H69 human SCLC in vivo model.

Two million NCI-H69 SCLC cells in 100 μl were mixed with Matrigel (Thermo Fisher Scientific) at 1:1 ratio and then injected into both hind flanks of NSG mice. When the majority of tumors were palpable, mice were randomized and treated with an isotype control, anti-CD47, anti-GD2 or the combination of anti-CD47 and anti-GD2 as described for the models above. Tumors were measured with digital calipers twice a week, and mice were euthanized when tumors reached the volume threshold set by institutional protocol.

Syngeneic TH-MYCN in vivo model.

De novo tumors from TH-MYCN mice were harvested and dissociated into single cells, and 1×10^6 cells were injected subcutaneously in the right flank of female 129X1/SvJ mice (8 weeks old). The cells were resuspended in a 1:1 solution of Neurobasal media (Gibco) and Geltrex (Gibco) before injection. After tumor formation, tumor size was measured twice a week. Mice began treatment when tumors reached a volume of ~700 mm^3. Mice were treated by intraperitoneal injection with 50 μg of murine anti-GD2 antibody (14G2a; see

details above), 30 mg kg^{-1} of murine CD47 blocker (ALX301) or a combination of both twice a week for a total of 3 weeks. Mice were sacrificed when the tumor size reached 2 cm in one direction. For macrophage depletion, mice were pre-treated by intravenous injection with 100 μl of clodronate liposomes (Liposoma), followed by 400 μg of anti-CSF1R (Bio X Cell, AFS98) by intraperitoneal injection 2 d later and then enrolled in treatment groups. Mice were treated with 400 μg of anti-CSF1R three times per week for the 3 weeks of treatment. For the toxicity experiment, non-tumor-bearing 129X1/SvJ mice were treated with PBS, 50 μg of murine anti-GD2 antibody (14G2a), 30 mg kg^{-1} of murine CD47 blocker (ALX301) or a combination of both twice a week for a total of three doses. Weight was assessed serially, and behavioral analysis was performed as described below. At the end of the experiment, mice were sent for necropsy to assess tissues by a board-certified veterinary pathologist (details described below).

Behavioral analysis.

To investigate neurological effects of treatment, the CatWalk gait analysis system (Noldus) was used. The apparatus consists of a glass walkway with opaque black siding that is internally illuminated with fluorescent lights via one of the long edges of the glass floor. As the mouse traverses the glass floor, the footprints cause the light to be reflected downward and are recorded by a camera positioned underneath the glass and relayed to an adjacent computer. A detailed description of the CatWalk method was previously published[31]. All tests were run in a dark room. Animals were tested at indicated time points and received no prior training on the CatWalk. Three successful runs (characterized by variation under 60%, lasting no more than 5 s and consistent movement) were processed with CatWalk XT 9.0 software. Parameters measured are described on the Noldus website (www.noldus.com): swing speed, stride length and regularity index.

Neutrophil depletion.

The metastatic CHLA255 model was used as described above. First, 500 μg of anti-Ly6G (clone 1A8, Bio X Cell) was injected intaperitoneally every other day throughout the course of treatment, beginning 2 d before the start of treatment. To confirm depletion of neutrophils, peripheral blood was collected on the final day of treatment, ACK lysed and stained with anti-Ly6G/Ly6C (clone RB6–8C5, Thermo Fisher Scientific).

Phenotyping of intratumoral macrophages.

For osteosarcoma, 1 million MG63.3 tumor cells were injected as described above and allowed to grow for 3 weeks. For neuroblastoma, 1 million CHLA255 tumor cells were injected into the flank in 100 μl of a 1:1 mix of PBS and Matrigel and allowed to grow for 19 d. Antibody treatment was administered intraperitoneally with 400 μg of IgG control, 300 μg of anti-GD2 (dinutuximab), 400 μg of anti-CD47 (B6H12) or the combination of anti-GD2 and anti-CD47 three times per week for 1 week. Tumor tissues were excised and split into half (other half used for IHC; see below). One half was homogenized into single cells in cRPMI with a Miltenyi gentleMACS. Digested tumors were subsequently passed through a 70-μM filter and adjusted to a concentration of 10×10^6 cells per milliliter for staining in FACS buffer. Dead cells were stained with Live/Dead Violet (Thermo Fisher Scientific) in 1 ml of PBS. Cells were subsequently blocked with 2 μl of TruStain FcX Fc

receptor blocking antibody (BioLegend) for 10 min on ice. Cell suspensions were washed and resuspended in FACS buffer with the following fluorophore-labeled antibodies for 30 min on ice: CD163-BV421, CD11c-BV510, BV605-CD86, CD11b-BV650, I-A/I-E-BV711, Ly6C-BV785, CD45-Spark Blue 550, PD-L1-PerCP-Cy5.5, CD80, PerCP-ef710, Ly6G-PE-Cy7, CD68-AF647, CD206-AF700 and F4/80-APC-Cy7. The proportions of M2-like TAMs (CD45$^+$CD11b$^+$F4/80$^+$CD163$^+$CD206$^+$) within the tumor tissues of mice receiving different treatments were analyzed.

IHC and analysis.

Tumors were harvested as above. Formalin-fixed, paraffin-embedded xenograft tumor sections were used. GFP (Abcam, ab6556, 1:1,500) and F4/80 (Cell Signaling Technology, D2S9R) staining was performed manually, and iNOS (Novus, NB300–605SS, 1:500 dilution) staining was performed using the Ventana Discovery platform. In brief, tissue sections were incubated in either 6 mM citrate buffer (GFP and F4/80) or Tris EDTA buffer (iNOS) (cell conditioning 1 standard) at 100 °C for 25 min (GFP/F480) or 95 °C for 1 h (iNOS) to retrieve antigenicity, followed by incubation with the respective primary antibody for 1 h. Bound primary antibodies were incubated with the respective secondary antibodies (Vector Laboratories or Jackson Laboratory) with 1:500 dilution, followed by UltraMap HRP and Vectore Lab (GFP/F480) or ChromoMap DAB (iNOS) detection. For IHC analysis, lung macrometastases (>200 μm) were identified based on GFP positivity. F4/80 and iNOS positivity was analyzed for each tumor (each area ~3 mm^2). F4/80 and iNOS IHC positivity scores were automatically quantified in the regions of interest with Aperio ImageScope software. Regions of interest were randomly selected within the tumor to exclude macrophages present in the normal tissue around the tumor.

Histology for toxicity analysis.

The tissues assessed include salivary glands, liver, spleen, kidney, pancreas, heart, lung, tongue, trachea, esophagus, thyroid glands, haired skin, brown adipose tissue, white adipose tissue, cerebrum cerebellum, eyes, spinal cord, peripheral nerves, stomach, small intestine, large intestine, ovaries, uterus, long bone, bone marrow, vertebrae, epaxial muscle and hypaxial muscle. Tissues were harvested and immersion-fixed in 10% neutral buffered formalin. The skull, vertebral column, long bones and ribs were decalcified with a ready-to-use solution (Cal-Ex II). After fixation, tissues were routinely processed, embedded in paraffin, sectioned at 5.0 μm and routinely stained with hematoxylin and eosin (H&E). Tissues were visualized with an Olympus BX43 upright bright-field microscope, and images were captured using an Olympus DP27 camera and cellSens software. Tissues were assessed in a blinded manner by a board-certified veterinary pathologist.

MRI.

One million MG63.3 tumor cells were injected as described above and allowed to grow for 3 weeks. At this time, mice underwent a baseline MRI. A second MRI was performed after antibody treatment with 300 μg of anti-GD2 (dinutuximab) and 400 μg anti-CD47 (B6H12) or 400 μg IgG control three times per week for 1 week. On the same day as the second MRI, mice received ferumoxytol intravenously at the dose of 0.5 mmol Fe per kilogram. Repeat MRI was performed 12 h after ferumoxytol injection. MRI studies were

performed on a 7T MR scanner (Bruker BioSpin) using a 2.9-cm-inner-diameter (4 cm active length) Millipede RF coil (ExtendMR) operating in quadrature and tuned to 298.06 MHz, specifically designed for high-field micro-imaging of the mouse, and the following pulse sequences with a field of view of 3 cm × 3 cm and a slice thickness of 0.75 mm: T2-weighted fast spin echo (FSE): repetition time (TR): 2,528 ms, echo time (TE): 33 ms and T2*-map multi-gradient echo: flip angle: 80°, TR: 999 ms and TE: 3, 7,12,16, 20, 25, 29, 33, 38 and 42 ms.

Mean T2* values of the tumors were analyzed using OsiriX software version 8.0.2 (Pixmeo SARL) to quantify tumor contrast enhancement. The slice with the largest cross-sectional area of the tumor in the T2-weighted FSE image volume was identified for each animal. The visible tumor boundary was defined within that slice. The mean T2* value within the visible tumor boundary was calculated for each animal. T2* means were averaged across control and treated animal groups at each time point.

Analysis of RNA expression data.

Publicly available RNA expression and relevant clinical prognostic parameters were obtained from the R2: Genomics Analysis and Visualization Platform (https://hgserver1.amc.nl/cgi-bin/r2/main.cgi) from following datasets: TARGET, Westermann and SEQC for neuroblastoma and Kuijjer for osteosarcoma. Expression data corresponding to SCLC were obtained from reference[67]. Analysis of correlation between clinical parameters and gene expression in neuroblastoma datasets was done using available sample annotation. Correlation between Myc levels and CD47 in osteosarcoma and SLCL was done by comparing the top ~20% of samples with higher levels of expression of any Myc family gene (*MYC*, *MYCL* and *MYCN*) versus the lowest 40–50%, depending on distribution of the sample.

Statistical analysis.

Data analysis and visualization was performed using Excel version 16.14.1 (Microsoft) and Prism 8.4 (GraphPad). Graphs represent either group mean values ± s.d. (for in vitro experiments) or ± s.e.m. (for in vivo experiments) or individual values. For in vitro studies, statistical comparisons were made with either unpaired *t*-tests when comparing two groups or one-way ANOVA with multiple comparison correction when comparing more than two groups. For in vivo studies, survival curves were compared with the log-rank test; tumor growth was compared with repeated-measures ANOVA; and the Mann–Whitney test was used to compare two groups. $P < 0.05$ was considered statistically significant. P values are denoted with asterisks: $P > 0.05$, NS; *$P < 0.05$; **$P < 0.01$; ***$P < 0.001$; and ****$P < 0.0001$.

Reporting Summary.

Further information on research design is available in the Nature Research Reporting Summary linked to this article.

Data availability

All statistics for the main and extended data figures are provided in the Supplementary Information. Source data for Figs. 1–3 and 5 and 6 and Extended Data Figs. 1–2 and 4–9 are supplied. The unprocessed gel blot image for Extended Data Fig. 3 is also provided. Source data are provided with this paper.

Extended Data
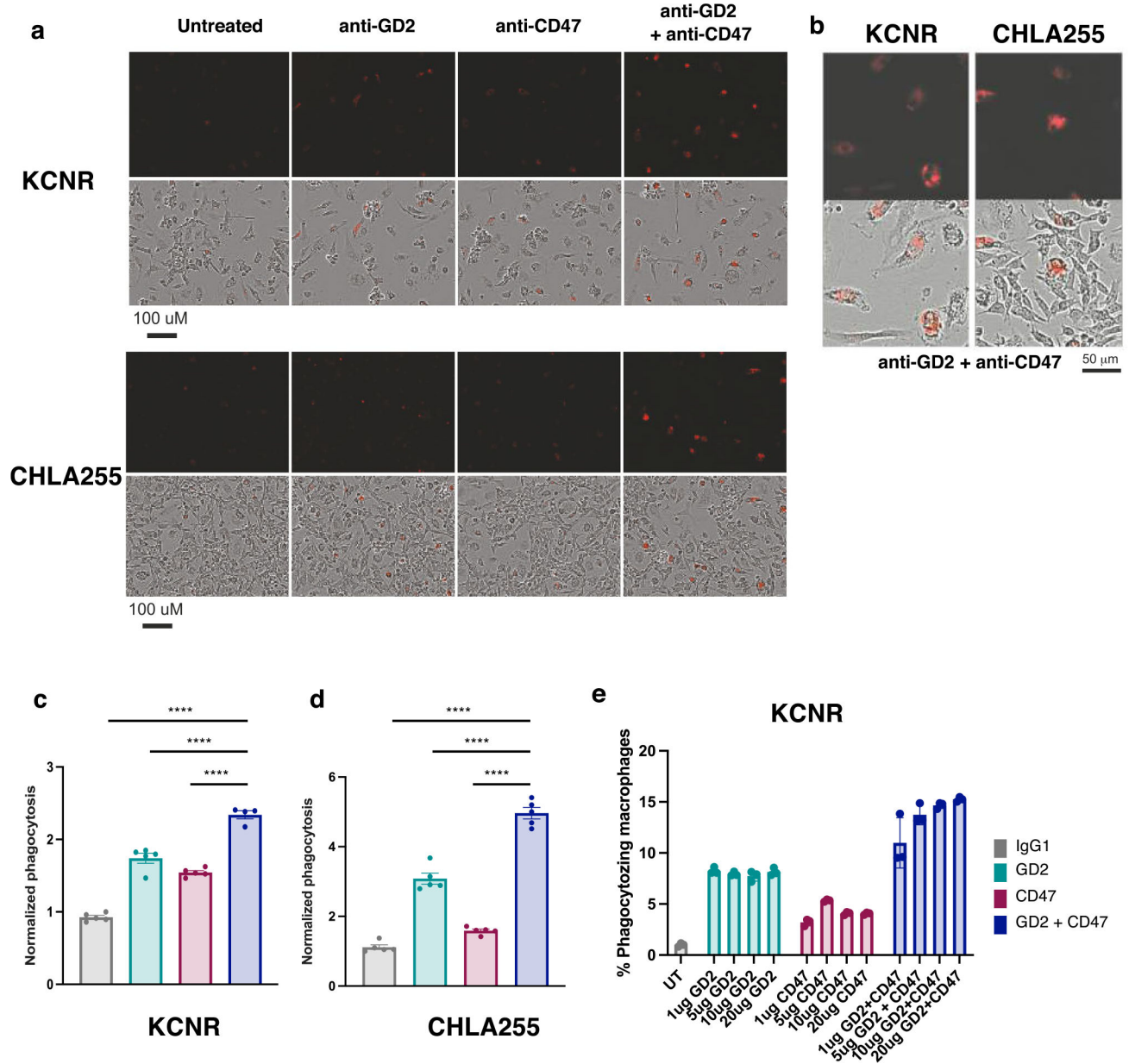
Extended Data Fig. 1 |. anti-GD2 and anti-CD47 synergize to promote tumor cell phagocytosis. a-b, Representative Images of Incucyte based live cell phagocytosis assay. a, pHrodo red labeled KCNR (top) or CHLA255 (bottom) neuroblastoma cells were co-cultured with

human blood derived macrophages in the presence of anti-GD2 mAb, anti-CD47 mAb or dual treatment. Red indicative of tumor cell phagocytosis. Images were obtained after 24 hours of co-culture. **b**, Magnified image of cells shown in **a**. **c-d**, Quantification of phagocytosis normalized to the phagocytosis in the untreated control for each cell line, **c**, KCNR (Untreated vs. GD2+CD47 p = 2.9E-14, GD2 vs. GD2+CD47 p = 5.4681E-10, CD47 vs. GD2+CD47 p = 1.13E-12) **d**, CHLA255 (Untreated vs. GD2+CD47 p = 3.3E-14, GD2 vs. GD2+CD47 p = 2.128E-12, CD47 vs. GD2+CD47 p = 3.3E-14). Data are mean values +/− s.e.m. of five experimental replicates. Experiment was performed one time. **e**, Flow-based phagocytosis assay of KCNR neuroblastoma cells co-cultured with human blood derived macrophages in the presence of different concentrations of anti-GD2 mAb, anti-CD47 mAb or dual treatment. % phagocytosing macrophages are reported. Data are mean values +/− s.d. of three experimental replicates. Experiment was performed one time. Statistical comparisons performed with one-way ANOVA with multiple comparisons correction, *P < 0.05, **P < 0.01, ***P < 0.001, ****P < 0.0001, ns P>0.05.
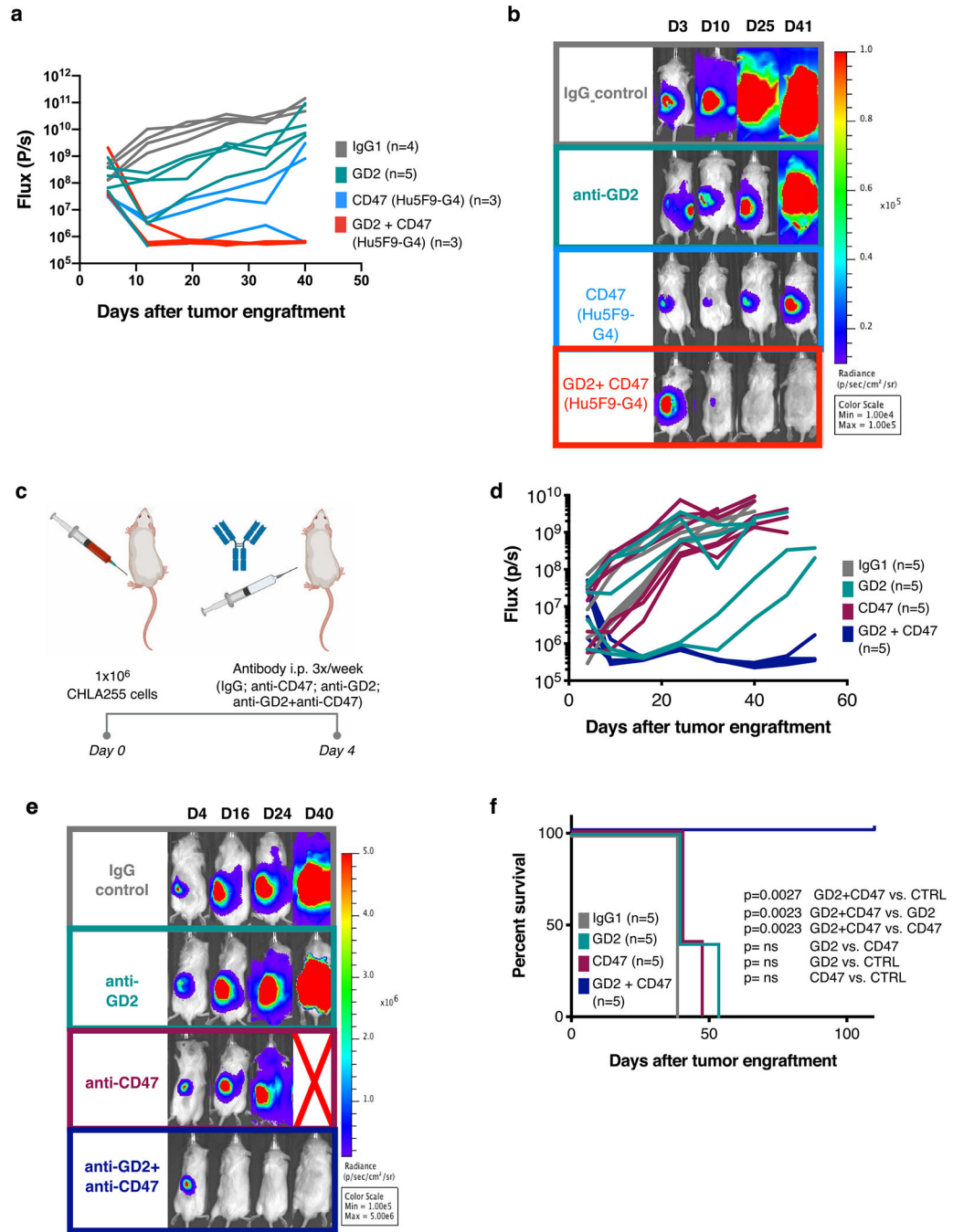
Extended Data Fig. 2 |. Anti-CD47 and anti-GD2 synergize to mediate significant anti-tumor activity in orthotopic models of neuroblastoma.
One million KCNR neuroblastoma cells expressing GFP-luciferase were implanted into the renal capsule and treated four days later with IgG control, anti-G2 mAb, anti-CD47 (magrolimab, Hu5F9-G4) mAb or dual anti-GD2/anti-CD47 (Hu5F9-G4) every other day for three doses as in Fig. 1c. **a**, Quantification of tumor progression for each individual mouse as measured by flux values acquired via bioluminescence (BLI) photometry. **b**, BLI images of representative mice from each treatment group at different time points.

Experiment was performed one time. N = 4 mice for IgG, and N = 5 for anti-GD2 per group and those groups are the same as in Fig. 1c–f. N=3 for anti-CD47 and anti-CD47 + anti-GD2 **c**, One million CHLA255 neuroblastoma cells expressing GFP-luciferase cells were implanted into the renal capsule in NSG mice. Four days later, mice were injected with IgG control, anti-GD2 mAb, anti-CD47 mAb or dual anti-GD2/anti-CD47 treatment every other day for three doses. **d**, Quantification of tumor progression for each individual mouse as measured by flux values acquired via BLI photometry. **e**, BLI images of representative mice from each treatment group shown in **d** at different time points. Red cross indicates deceased mouse. **f**, Survival curves for mice bearing tumors shown in **d**. d-f, Representative data from three independent experiments with N = 5 mice per group. All survival curves were compared using the Log-rank test (two-tailed).

a, Schematic of ALX301: Murine IgG1 containing a N297A mutation was fused to a mutated SIRPα capable of binding murine CD47 with enhanced affinity. **b**, Purified ALX301 was detected on 4–20% Tris-glycine gel in non-reducing (NR) and reducing (R) buffer. ALX301 runs slightly larger than the expected 76.16 kDa (NR) and 38.038 kDa (R). **c**, ALX301 was immobilized on GLC sensor chip (Bio-rad). Recombinant mouse CD47 protein was injected as analyte over the chip at 5 concentrations, 3-fold dilution (100nM,

Extended Data Fig. 3 |. Expression and affinity of ALX301, an engineered molecule capable of blocking murine CD47.

33.3nM, 11.1nM, 3.7nM, 1.2nM). Using Langmuir binding model for curve fitting, the binding of ALX301 to mouse SIRPα was determined to be 3.41nM. Association rate (ka), dissociation rate (kd), affinity (KD). **b-c** were performed one time.
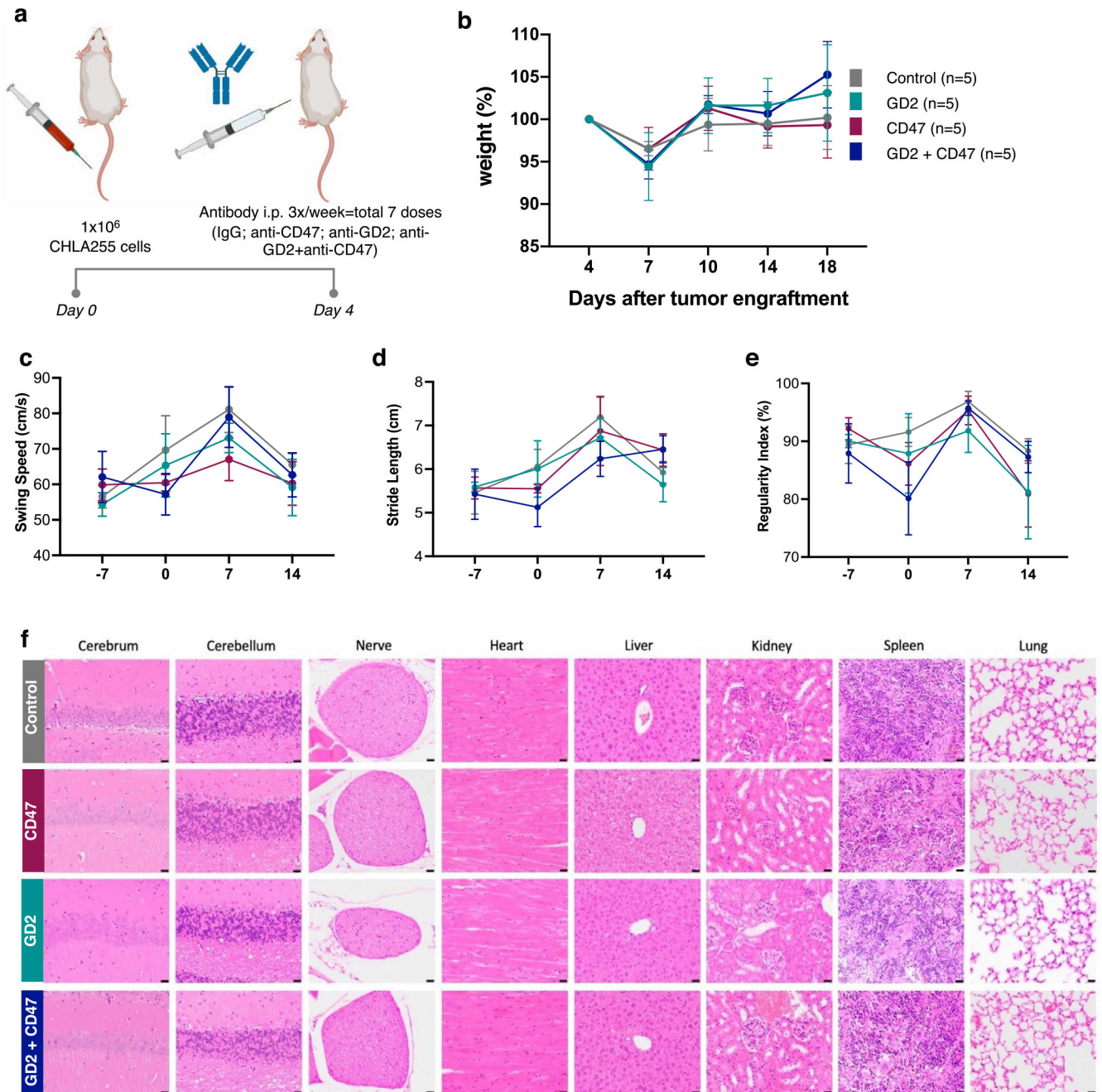

Extended Data Fig. 4 |. Absence of toxicity of anti-GD2 and anti-CD47 treated mice in a model of metastatic neuroblastoma.

**a**, One million CHLA255 neuroblastoma cell were injected in the tail vein of the mice. After 4 days mice were treated intraperitoneally with PBS (control), anti-GD2, anti-CD47 or the combination of anti-GD2 and anti-CD47 3x/week for a total of 7 doses. **b**, Weight was

serially recorded. **c-e**, CatWalk gait analysis was performed at indicated time points and **c**, swing speed, **d**, stride length and **e**, regularity index are reported from mice treated as in **a**. Data shown are mean values +/− s.e.m. n = 5 mice per group. Experiment was performed one time. **f**, Hematoxylin and eosin (H&E) stained sections of all organs examined were within normal limits as assessed by brightfield microscopy. Shown are sections of cerebrum, cerebellum, peripheral nerve, heart, liver, kidney, spleen, and lung of animals from mice treated as in **a**. Magnification: 40x, Scale bars: 20μm.
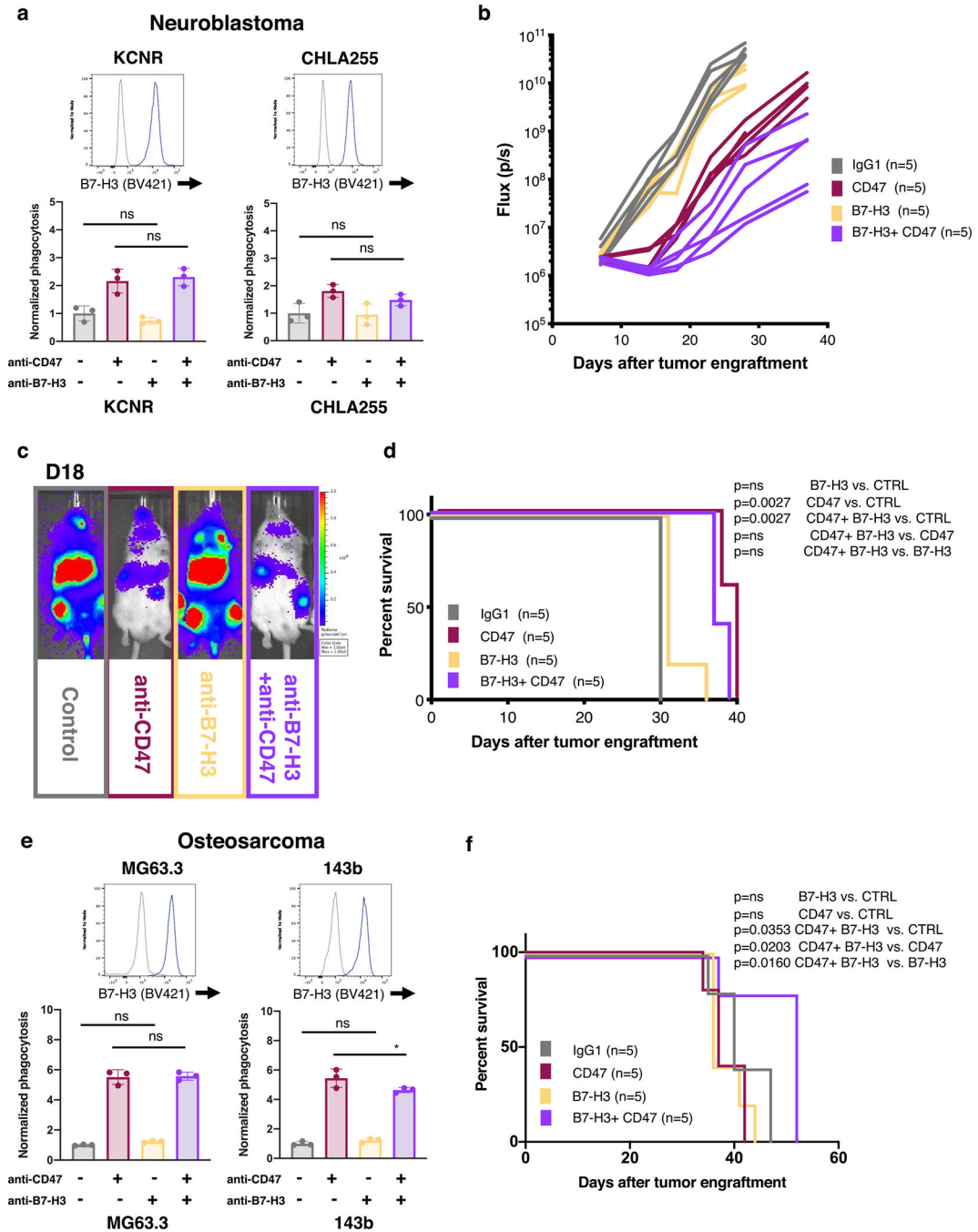
Extended Data Fig. 5 |. Lack of synergy of anti-B7-H3 with anti-CD47 in xenograft models of neuroblastoma or osteosarcoma.

a, Graphs show flow cytometry-based quantification of phagocytosis of neuroblastoma cell lines co-cultured with human blood derived macrophages in the presence of anti-CD47 mAb, anti-B7-H3 mAb, or dual treatment, compared with untreated control; results normalized to the phagocytosis in the untreated control for each cell line and blood donor. Shown are mean values +/− s.d. of three experimental replicates. Statistical comparisons performed with one-way ANOVA with multiple comparisons correction (KCNR: control vs. anti-B7-H3 $p = 0.9643$, anti-CD47 vs. anti-B7-H3 and anti-CD47 $p = 0.9976$; CHLA255: control vs. anti-B7-H3 $p>0.9999$, anti-CD47 vs. anti-B7-H3 and anti-CD47 $p = 0.8519$). Representative data from at least three experiments with three different blood donors. Inset: B7-H3 expression as assessed by flow cytometry on respective cell lines. b, One million CHLA255 neuroblastoma cells were engrafted into NSG mice by tail-vein injection. On D+4, mice were treated with IgG control, anti-CD47 mAb, anti-B7-H3 mAb, or anti-B7-H3+anti-CD47 every other day for three doses. Quantification of tumor progression for each individual mouse as measured by flux values acquired via BLI photometry. c, BLI images of representative mice from each treatment group shown in b at one time point. d, Survival curves for mice bearing tumors shown in b. N = 5 mice per group, performed one time. Survival curves were compared using the Log-rank test (two-tailed). e, Graph shows flow cytometry-based quantification of phagocytosis of osteosarcoma cell lines co-cultured with human blood derived macrophages; results normalized to the phagocytosis in the untreated control for each cell line and blood donor. Shown are mean values +/− s.d. of three experimental replicates. Statistical comparisons performed as in a. Representative data from at least three experiments with three different blood donors. Inset: B7-H3 expression as assessed by flow cytometry on respective cell lines. f, Survival curves for mice that received hind leg injection of 1e6 MG63.3 cells and treated on D+7 with indicated antibodies 3x/week for four weeks. N = 5 mice per group, performed one time. Survival curves were compared using the Log-rank test (two-tailed). *P < 0.05, ns P>0.05.
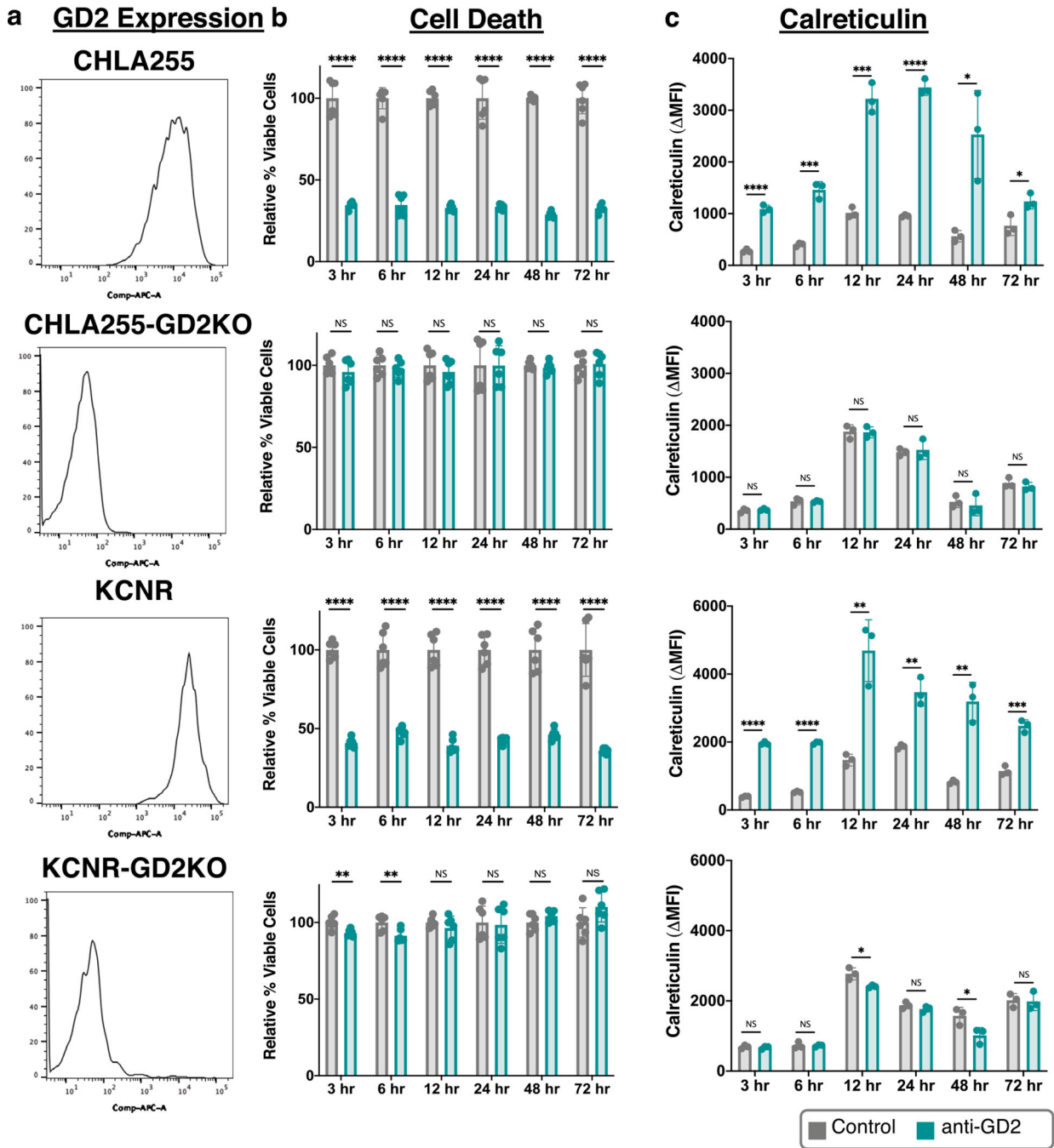
Extended Data Fig. 6 |. upregulation of 'Eat me' signal calreticulin and induction of cell death by ligation with anti-GD2 mAb on neuroblastoma cell lines.
**a**, Flow cytometric analysis of the levels of expression of GD2 on the surface of neuroblastoma cell lines CHLA255 and KCNR and their GD2-KO (*B4GALNT1* KO) versions. **b**, Flow-based quantification of cell viability. Neuroblastoma cell lines and their GD2-KO versions were incubated with anti-GD2 mAb for the indicated times at 37 degrees and stained with DAPI. Percent of DAPI- populations were normalized to the untreated control for each cell line. Shown are mean values +/− s.d. of 6 experimental replicates.

(CHLA255: 3hr p = 4.17E-08, 6hr p = 6.5044E-09, 12hr p = 1.2983E-11, 24hr p = 1.9094E-07, 48hr p = 7E-15, 72hr p = 1.2397E-08; CHLA255 GD2 KO: 3hr p = 0.3013, 6hr p = 0.506, 12hr p = 0.4125, 24hr p = 0.983, 48hr p = 0.4263, 72hr p = 0.8453; KCNR: 3hr p = 3.75E-10, 6hr p = 7.0881E-07, 12hr p = 1.1406E-07, 24hr p = 4.2986E-08, 48hr p = 2.6777E-06, 72hr p = 2.9544E-06; KCNR GD2 KO: 3hr p = 0.0059, 6hr p = 0.0083, 12hr p = 0.3223, 24hr p = 0.8197, 48hr p = 0.1443, 72hr p = 0.1002). **c**, Graph shows flow cytometric quantification of the expression of calreticulin (MFI) on the surface of live neuroblastoma cell lines treated as in **b**. Shown are mean values +/− s.d. of 3 experimental replicates. CHLA255: 3hr p = 6.57E-05, 6hr p = 0.0004, 12hr p = 0.0002, 24hr p = 9.2150E-06, 48hr p = 0.0167, 72hr p = 0.027; CHLA255 GD2 KO: 3hr p = 0.4701, 6hr p = 0.9563, 12hr p = 0.9024, 24hr p = 0.7235, 48hr p = 0.6415, 72hr p = 0.4069; KCNR: 3hr p = 7.41E-07, 6hr p = 7.4552E-07, 12hr p = 0.0038, 24hr p = 0.0024, 48hr p = 0.0019, 72hr p = 0.0005; KCNR GD2 KO: 3hr p = 0.671, 6hr p = 0.9445, 12hr p = 0.023, 24hr p = 0.2359, 48hr p = 0.0426, 72hr p = 0.8656. MFI was calculated as the difference between the MFI in the PE channel of the calreticulin stained sample and the MFI in the PE channel of an isotype stained sample from the same experimental condition. The full time-course experiment was performed twice and the twelve-hour timepoint shown is identical to Fig. 4h. **b-c**, Statistical comparisons performed with the unpaired t-test, *P < 0.05, **P < 0.01, ***P < 0.001, ****P < 0.0001, ns P>0.05.
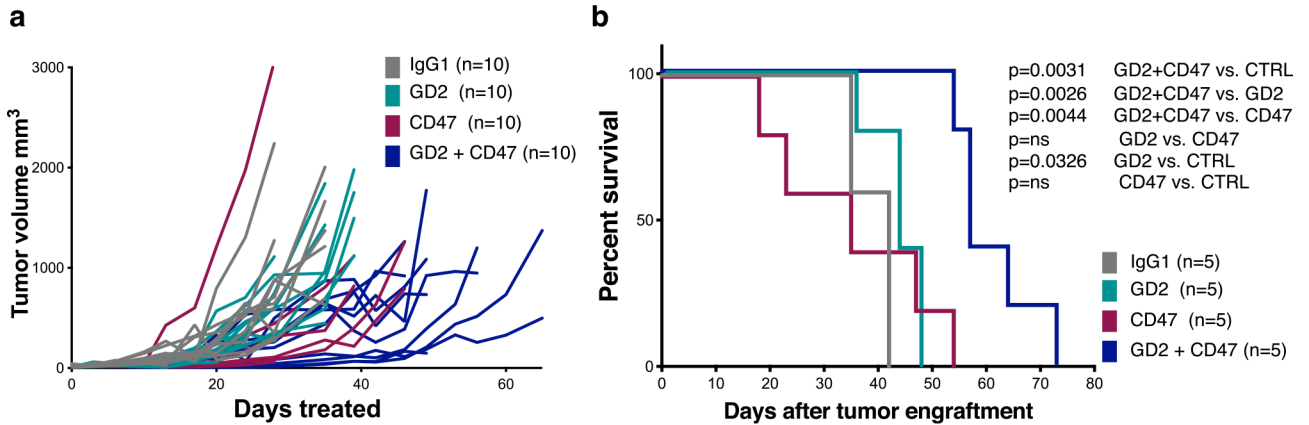
Extended Data Fig. 7 |. Anti-CD47 and anti-GD2 synergize to mediate significant anti-tumor activity in xenograft model of small cell lung cancer (SCLC).
a, NCI-H69 SCLC were engrafted on both flanks of NSG mice. Quantification of tumor growth for each individual tumor was assessed by caliper measurement. **b**, Survival curves for mice bearing tumors shown in **a**. Survival curves were compared using the Log-rank test (two-tailed). Representative of two independent experiments with n = 5 mice per group.
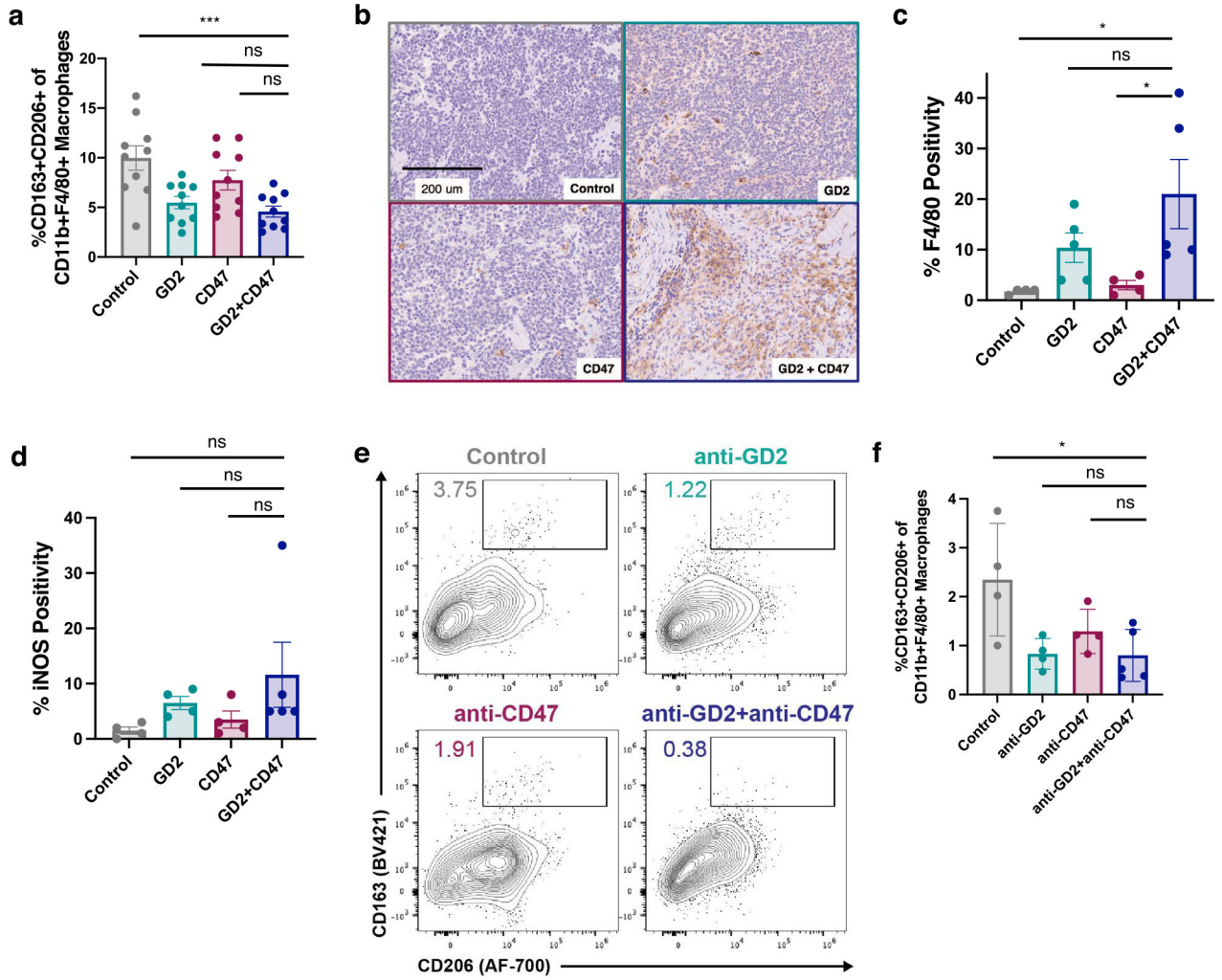
Extended Data Fig. 8 |. Anti-GD2 and anti-CD47 treatment leads to an increase in macrophage infiltration and reduction of M2 macrophages.

a, Flow cytometric analysis of M2 macrophages (defined as CD163+ and CD206+, gated on CD45+, CD11b+, F4/80 + macrophages) in osteosarcoma tumors treated as described in Fig. 6, pooled results from two independent experiments. Shown are mean values +/− s.em. of 10 experimental replicates. Control vs. GD2+CD47 p = 0.0007, CD47 vs. GD2+CD47 p = 0.0738, GD2 vs. GD2+CD47 p = 0.8869. **b-f**, CHLA255 neuroblastoma tumor cells were engrafted in the flank and allowed to grow for 19 days before initiation of treatment with IgG control, anti-GD2 mAb, anti-CD47 mAb or dual anti-GD2/anti-CD47. After one week of treatment, tumors were harvested for immunohistochemistry (IHC) and flow cytometric analysis. **b**, Representative IHC images showing detection of macrophages via staining with anti-F4/80 on tumors harvested from mice treated with indicated mAbs. **c**, Quantification of percent of positive F4/80 staining obtained from IHC analysis. Shown are mean values +/− s.e.m. of 4–5 biologic replicates. Control vs. GD2+CD47 p = 0.0281, CD47 vs. GD2+CD47 p = 0.0415, GD2 vs. GD2+CD47 p = 0.2804. **d**, Quantification of percent of positive iNOS staining obtained from IHC analysis. Shown are mean values +/− s.e.m. of 4–5 biologic replicates. Control vs. GD2+CD47 p = 0.2401, CD47 vs. GD2+CD47 p = 0.413, GD2

vs. GD2+CD47 p = 0.7487. **e-f**, Flow cytometric analysis of M2 macrophages (defined as CD163+ and CD206+, gated on CD45+, CD11b+, F4/80 + macrophages) in CHLA255 tumors. **e**, Representative flow plots and **f**, quantification of M2 macrophages. Shown are mean values +/− s.e.m. of 4–5 biologic replicates. Control vs. GD2+CD47 p = 0.0218, CD47 vs. GD2+CD47 p = 0.9999, GD2 vs. GD2+CD47 p = 0.7102. **b-f**, Experiment was performed one time. All statistical comparisons were made between groups with the one-way ANOVA with correction for multiple comparisons correction, *P < 0.05, **P < 0.01, ***P < 0.001, ****P < 0.0001, ns P>0.05.
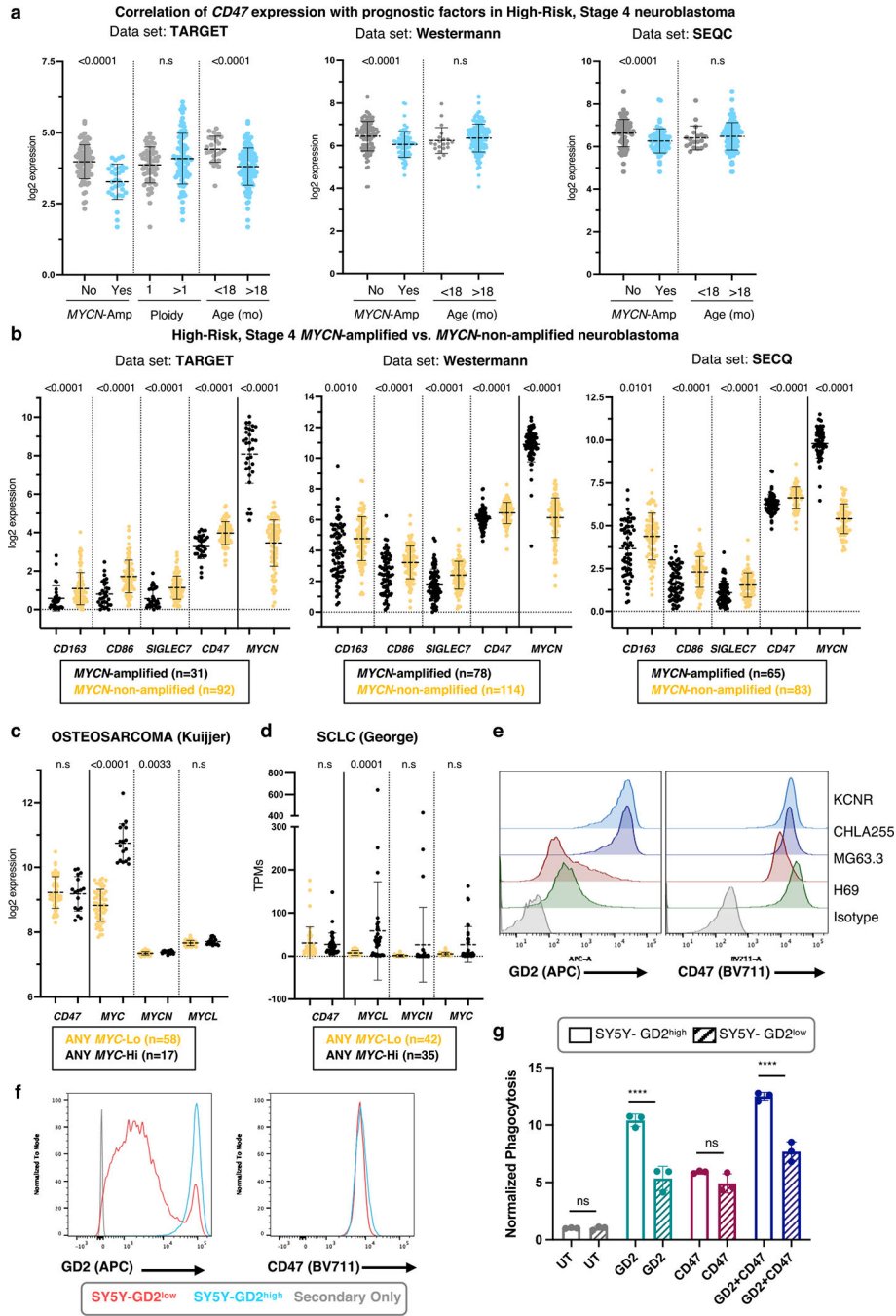
Extended Data Fig. 9 |. GD2 antigen density may determine response to anti-GD2/anti-CD47.
a, Expression levels of *CD47 mRNA* in samples from three different datasets of primary tumors from high-risk, stage 4 neuroblastoma stratified by MYCN status (amplified vs non-amplified), age at diagnosis, and ploidy (where available). **b**, Expression levels of *CD163*, *CD86,* and *SIGLEC7*, together with *CD47* and *MYCN* in samples from the same databases as in **a** grouped based on MYCN amplification status. **c-d**, Expression levels of *CD47* and *MYC* family genes in samples from osteosarcoma **c** or SCLC **d** primary tumors. Samples are stratified based on high or low expression of any of the three *MYC* family genes:

MYC, *MYCL* or *MYCN*. Dot plots represent log2 (**a-c**) or TPM (**d**) expression values. Error bars represent median ± s.d. Differences in gene expression levels between groups were calculated using the Mann-Whitney U test (unpaired, two-sided). **e**, Flow cytometric analysis of the expression of GD2 (top) and CD47 (bottom) on tumor cell lines used in *in vivo* models. **f**, Flow cytometric analysis of the expression of GD2 (top) and CD47 (bottom) on isogenic SH-SY5Y neuroblastoma GD2-low and GD2-high cell lines. **g**, Graphs show flow cytometry-based quantification of phagocytosis of SY5Y-GD2-low and SY5Y-GD2-high neuroblastoma cell lines co-cultured with human blood derived macrophages in the presence of anti-GD2 mAb, anti-CD47 mAb or dual treatment, compared with untreated control; results normalized to the phagocytosis in the untreated (UT) control for each cell line and blood donor. Shown are mean values +/− s.d. of three experimental replicates. SY5Y-GD2-high-UT vs. SY5Y-GD2-low-UT p>0.9999, SY5Y-GD2-high-GD2-treated vs. SY5Y-GD2-low-GD2-treated p = 5.1941E-07, SY5Y-GD2-high-CD47-treated vs. SY5Y-GD2-low-CD47-treated p = 0.5091, SY5Y-GD2-high-GD2+CD47-treated vs. SY5Y-GD2-low-GD2+CD47-treated p = 9.8567E-07. Representative data from two experiments performed with two different blood donors. Statistical comparisons performed with one-way ANOVA with multiple comparisons correction, *P < 0.05, **P < 0.01, ***P < 0.001, ****P < 0.0001, ns P>0.05.

Supplementary Material

Refer to Web version on PubMed Central for supplementary material.

Acknowledgements

References

1. Schulz G et al. Detection of ganglioside GD2 in tumor tissues and sera of neuroblastoma patients. Cancer Res. 44, 5914–5920 (1984). [PubMed: 6498849]

2. Long AH et al. Reduction of MDSCs with all-trans retinoic acid improves CAR therapy efficacy for sarcomas. Cancer Immunol. Res. 4, 869–880 (2016). [PubMed: 27549124]

3. Dobrenkov K, Ostrovnaya I, Gu J, Cheung IY & Cheung NK Oncotargets GD2 and GD3 are highly expressed in sarcomas of children, adolescents, and young adults. Pediatr. Blood Cancer 63, 1780–1785 (2016). [PubMed: 27304202]

4. Mount CW et al. Potent antitumor efficacy of anti-GD2 CAR T cells in H3-K27M+ diffuse midline gliomas. Nat. Med. 24, 572–579 (2018). [PubMed: 29662203]

5. Cheresh DA, Rosenberg J, Mujoo K, Hirschowitz L & Reisfeld RA Biosynthesis and expression of the disialoganglioside GD2, a relevant target antigen on small cell lung carcinoma for monoclonal antibody-mediated cytolysis. Cancer Res. 46, 5112–5118 (1986). [PubMed: 3019521]

6. Battula VL et al. Ganglioside GD2 identifies breast cancer stem cells and promotes tumorigenesis. J. Clin. Invest. 122, 2066–2078 (2012). [PubMed: 22585577]

7. Yu AL et al. Anti-GD2 antibody with GM-CSF, interleukin-2, and isotretinoin for neuroblastoma. N. Engl. J. Med. 363, 1324–1334 (2010). [PubMed: 20879881]

8. Ladenstein R et al. Interleukin 2 with anti-GD2 antibody ch14.18/CHO (dinutuximab beta) in patients with high-risk neuroblastoma (HR-NBL1/SIOPEN): a multicentre, randomised, phase 3 trial. Lancet Oncol. 19, 1617–1629 (2018). [PubMed: 30442501]

9. Cheung NK et al. Murine anti-GD2 monoclonal antibody 3F8 combined with granulocyte-macrophage colony-stimulating factor and 13-*cis*-retinoic acid in high-risk patients with stage 4 neuroblastoma in first remission. J. Clin. Oncol. 30, 3264–3270 (2012). [PubMed: 22869886]

10. Hobbie WL et al. Late effects in survivors of tandem peripheral blood stem cell transplant for high-risk neuroblastoma. Pediatr. Blood Cancer 51, 679–683 (2008). [PubMed: 18623215]

11. Suh E et al. Late mortality and chronic health conditions in long-term survivors of early-adolescent and young adult cancers: a retrospective cohort analysis from the Childhood Cancer Survivor Study. Lancet Oncol. 21, 421–435 (2020). [PubMed: 32066543]

12. Moreno L et al. Outcome of children with relapsed or refractory neuroblastoma: a meta-analysis of ITCC/SIOPEN European phase II clinical trials. Pediatr. Blood Cancer 64, 25–31 (2017). [PubMed: 27555472]

13. Hingorani P et al. Phase II study of antidisialoganglioside antibody, dinutuximab, in combination with GM-CSF in patients with recurrent osteosarcoma (AOST1421): a report from the Children's Oncology Group. J. Clin. Oncol. 38, 10508–10508 (2020).

14. Edelman M et al. The anti-disialoganglioside (GD2) antibody dinutuximab (D) for second-line treatment (2LT) of patients (pts) with relapsed/refractory small cell lung cancer (RR SCLC): results from part II of the open-label, randomized, phase II/III distinct study. J. Clin. Oncol. 38, 9017–9017 (2020).

15. Grant SC et al. Targeting of small-cell lung cancer using the anti-GD2 ganglioside monoclonal antibody 3F8: a pilot trial. Eur. J. Nucl. Med. 23, 145–149 (1996). [PubMed: 8925848]

16. Chao MP et al. Calreticulin is the dominant pro-phagocytic signal on multiple human cancers and is counterbalanced by CD47. Sci. Transl. Med. 2, 63ra94 (2010).

17. Jaiswal S et al. CD47 is upregulated on circulating hematopoietic stem cells and leukemia cells to avoid phagocytosis. Cell 138, 271–285 (2009). [PubMed: 19632178]

18. Sikic BI et al. First-in-human, first-in-class phase I trial of the anti-CD47 antibody Hu5F9-G4 in patients with advanced cancers. J. Clin. Oncol. 37, 946–953 (2019). [PubMed: 30811285]

19. Advani R et al. CD47 blockade by Hu5F9-G4 and rituximab in non-Hodgkin's lymphoma. N. Engl. J. Med. 379, 1711–1721 (2018). [PubMed: 30380386]

20. Chao MP et al. Anti-CD47 antibody synergizes with rituximab to promote phagocytosis and eradicate non-Hodgkin lymphoma. Cell 142, 699–713 (2010). [PubMed: 20813259]

21. Desai AV et al. Pharmacokinetics of the chimeric anti-GD2 antibody, ch14.18, in children with high-risk neuroblastoma. Cancer Chemother. Pharmacol. 74, 1047–1055 (2014). [PubMed: 25212536]

22. Weiss WA, Aldape K, Mohapatra G, Feuerstein BG & Bishop JM Targeted expression of *MYCN* causes neuroblastoma in transgenic mice. EMBO J. 16, 2985–2995 (1997). [PubMed: 9214616]

23. Sockolosky JT et al. Durable antitumor responses to CD47 blockade require adaptive immune stimulation. Proc. Natl Acad. Sci. USA 113, E2646–E2654 (2016). [PubMed: 27091975]

24. Willingham SB et al. The CD47-signal regulatory protein alpha (SIRPa) interaction is a therapeutic target for human solid tumors. Proc. Natl Acad. Sci. USA 109, 6662–6667 (2012). [PubMed: 22451913]

25. Lammie G, Cheung N, Gerald W, Rosenblum M & Cordoncardo C Ganglioside gd(2) expression in the human nervous-system and in neuroblastomas - an immunohistochemical study. Int. J. Oncol. 3, 909–915 (1993). [PubMed: 21573452]

26. Svennerholm L et al. Gangliosides and allied glycosphingolipids in human peripheral nerve and spinal cord. Biochim. Biophys. Acta 1214, 115–123 (1994). [PubMed: 7918590]

27. Zhang S et al. Selection of tumor antigens as targets for immune attack using immunohistochemistry: I. Focus on gangliosides. Int J. Cancer 73, 42–49 (1997). [PubMed: 9334808]

28. Ngamukote S, Yanagisawa M, Ariga T, Ando S & Yu RK Developmental changes of glycosphingolipids and expression of glycogenes in mouse brains. J. Neurochem. 103, 2327–2341 (2007). [PubMed: 17883393]

29. Xiao WH, Yu AL & Sorkin LS Electrophysiological characteristics of primary afferent fibers after systemic administration of anti-GD2 ganglioside antibody. Pain 69, 145–151 (1997). [PubMed: 9060025]

30. Sorkin LS et al. Anti-GD$_2$ with an FC point mutation reduces complement fixation and decreases antibody-induced allodynia. Pain 149, 135–142 (2010). [PubMed: 20171010]

31. Hamers FP, Lankhorst AJ, van Laar TJ, Veldhuis WB & Gispen WH Automated quantitative gait analysis during overground locomotion in the rat: its application to spinal cord contusion and transection injuries. J. Neurotrauma 18, 187–201 (2001). [PubMed: 11229711]

32. Loo D et al. Development of an Fc-enhanced anti-B7-H3 monoclonal antibody with potent antitumor activity. Clin. Cancer Res. 18, 3834–3845 (2012). [PubMed: 22615450]

33. Crocker PR, Paulson JC & Varki A Siglecs and their roles in the immune system. Nat. Rev. Immunol. 7, 255–266 (2007). [PubMed: 17380156]

34. Wei JS et al. Clinically relevant cytotoxic immune cell signatures and clonal expansion of T-cell receptors in high-risk *MYCN*-not-amplified human neuroblastoma. Clin. Cancer Res. 24, 5673–5684 (2018). [PubMed: 29784674]

35. Asgharzadeh S et al. Clinical significance of tumor-associated inflammatory cells in metastatic neuroblastoma. J. Clin. Oncol. 30, 3525–3532 (2012). [PubMed: 22927533]

36. Avril T, Floyd H, Lopez F, Vivier E & Crocker PR The membrane-proximal immunoreceptor tyrosine-based inhibitory motif is critical for the inhibitory signaling mediated by Siglecs-7 and −9, CD33-related Siglecs expressed on human monocytes and NK cells. J. Immunol. 173, 6841–6849 (2004). [PubMed: 15557178]

37. Yamaji T, Mitsuki M, Teranishi T & Hashimoto Y Characterization of inhibitory signaling motifs of the natural killer cell receptor Siglec-7: attenuated recruitment of phosphatases by the receptor is attributed to two amino acids in the motifs. Glycobiology 15, 667–676 (2005). [PubMed: 15703304]

38. Tsao CY et al. Anti-proliferative and pro-apoptotic activity of GD2 ganglioside-specific monoclonal antibody 3F8 in human melanoma cells. Oncoimmunology 4, e1023975 (2015). [PubMed: 26405581]

39. Doronin II et al. Ganglioside GD2 in reception and transduction of cell death signal in tumor cells. BMC Cancer 14, 295 (2014). [PubMed: 24773917]

40. Gardai SJ et al. Cell-surface calreticulin initiates clearance of viable or apoptotic cells through *trans*-activation of LRP on the phagocyte. Cell 123, 321–334 (2005). [PubMed: 16239148]

41. Lo M et al. Effector-attenuating substitutions that maintain antibody stability and reduce toxicity in mice. J. Biol. Chem. 292, 3900–3908 (2017). [PubMed: 28077575]

42. Roth M et al. Ganglioside GD2 as a therapeutic target for antibody-mediated therapy in patients with osteosarcoma. Cancer 120, 548–554 (2014). [PubMed: 24166473]

43. Gibson TM et al. Temporal patterns in the risk of chronic health conditions in survivors of childhood cancer diagnosed 1970–99: a report from the Childhood Cancer Survivor Study cohort. Lancet Oncol. 19, 1590–1601 (2018). [PubMed: 30416076]

44. Jaffe N, Puri A & Gelderblom H Osteosarcoma: evolution of treatment paradigms. Sarcoma 2013, 203531 (2013). [PubMed: 23781130]

45. Majzner RG et al. Assessment of programmed death-ligand 1 expression and tumor-associated immune cells in pediatric. Cancer Tissues Cancer 123, 3807–3815 (2017). [PubMed: 28608950]

46. Yoshida S et al. Ganglioside G$_{D2}$ in small cell lung cancer cell lines: enhancement of cell proliferation and mediation of apoptosis. Cancer Res. 61, 4244–4252 (2001). [PubMed: 11358851]

47. Rudin CM et al. Pembrolizumab or placebo plus etoposide and platinum as first-line therapy for extensive-stage small-cell lung cancer: randomized, double-blind, phase III KEYNOTE-604 study. J. Clin. Oncol. 38, 2369–2379 (2020). [PubMed: 32468956]

48. Aghighi M et al. Magnetic resonance imaging of tumor-associated macrophages: clinical translation. Clin. Cancer Res. 24, 4110–4118 (2018). [PubMed: 29764855]

49. Wiebel M et al. Surface expression of the immunotherapeutic target G_{D2} in osteosarcoma depends on cell confluency. Cancer Rep. (Hoboken) 4, e1394 (2021). [PubMed: 33811471]

50. Slart R, Yu AL, Yaksh TL & Sorkin LS An animal model of pain produced by systemic administration of an immunotherapeutic anti-ganglioside antibody. Pain 69, 119–125 (1997). [PubMed: 9060021]

51. Song L et al. Vα24-invariant NKT cells mediate antitumor activity via killing of tumor-associated macrophages. J. Clin. Invest. 119, 1524–1536 (2009). [PubMed: 19411762]

52. Chen Y, Zhao B & Wang X Tumor infiltrating immune cells (TIICs) as a biomarker for prognosis benefits in patients with osteosarcoma. BMC Cancer 20, 1022 (2020). [PubMed: 33087099]

53. Best SA et al. Harnessing natural killer immunity in metastatic SCLC. J. Thorac. Oncol. 15, 1507–1521 (2020). [PubMed: 32470639]

54. White P, Liebhaber SA & Cooke NE 129×1/SvJ mouse strain has a novel defect in inflammatory cell recruitment. J. Immunol. 168, 869–874 (2002). [PubMed: 11777984]

55. Shan D, Ledbetter JA & Press OW Signaling events involved in anti-CD20-induced apoptosis of malignant human B cells. Cancer Immunol. Immunother. 48, 673–683 (2000). [PubMed: 10752475]

56. Mohanty S, Aghighi M, Yerneni K, Theruvath JL & Daldrup-Link HE Improving the efficacy of osteosarcoma therapy: combining drugs that turn cancer cell 'don't eat me' signals off and 'eat me' signals on. Mol. Oncol. 13, 2049–2061 (2019). [PubMed: 31376208]

57. Barkal AA et al. CD24 signalling through macrophage Siglec-10 is a target for cancer immunotherapy. Nature 572, 392–396 (2019). [PubMed: 31367043]

58. Wang J et al. Siglec-15 as an immune suppressor and potential target for normalization cancer immunotherapy. Nat. Med. 25, 656–666 (2019). [PubMed: 30833750]

59. Siglec-15: an attractive immunotherapy target. Cancer Discov. 10, 7–8 (2020).

60. Fisher GA et al. A phase Ib/II study of the anti-CD47 antibody magrolimab with cetuximab in solid tumor and colorectal cancer patients. J. Clin. Oncol. 38, 114–114 (2020).

61. Majzner RG et al. Tuning the antigen density requirement for CAR T-cell activity. Cancer Discov. 10, 702–723 (2020). [PubMed: 32193224]

62. Lynn RC et al. c-Jun overexpression in CAR T cells induces exhaustion resistance. Nature 576, 293–300 (2019). [PubMed: 31802004]

63. Weiskopf K et al. Engineered SIRPα variants as immunotherapeutic adjuvants to anticancer antibodies. Science 341, 88–91 (2013). [PubMed: 23722425]

64. Gholamin S et al. Disrupting the CD47-SIRPα anti-phagocytic axis by a humanized anti-CD47 antibody is an efficacious treatment for malignant pediatric brain tumors. Sci. Transl. Med. 9, eaaf2968 (2017). [PubMed: 28298418]

65. Gray MA et al. Targeted glycan degradation potentiates the anticancer immune response in vivo. Nat. Chem. Biol. 16, 1376–1384 (2020). [PubMed: 32807964]

66. Wu HW et al. Anti-CD105 antibody eliminates tumor microenvironment cells and enhances anti-GD2 antibody immunotherapy of neuroblastoma with activated natural killer cells. Clin. Cancer Res. 25, 4761–4774 (2019). [PubMed: 31068371]

67. George J et al. Comprehensive genomic profiles of small cell lung cancer. Nature 524, 47–53 (2015). [PubMed: 26168399]
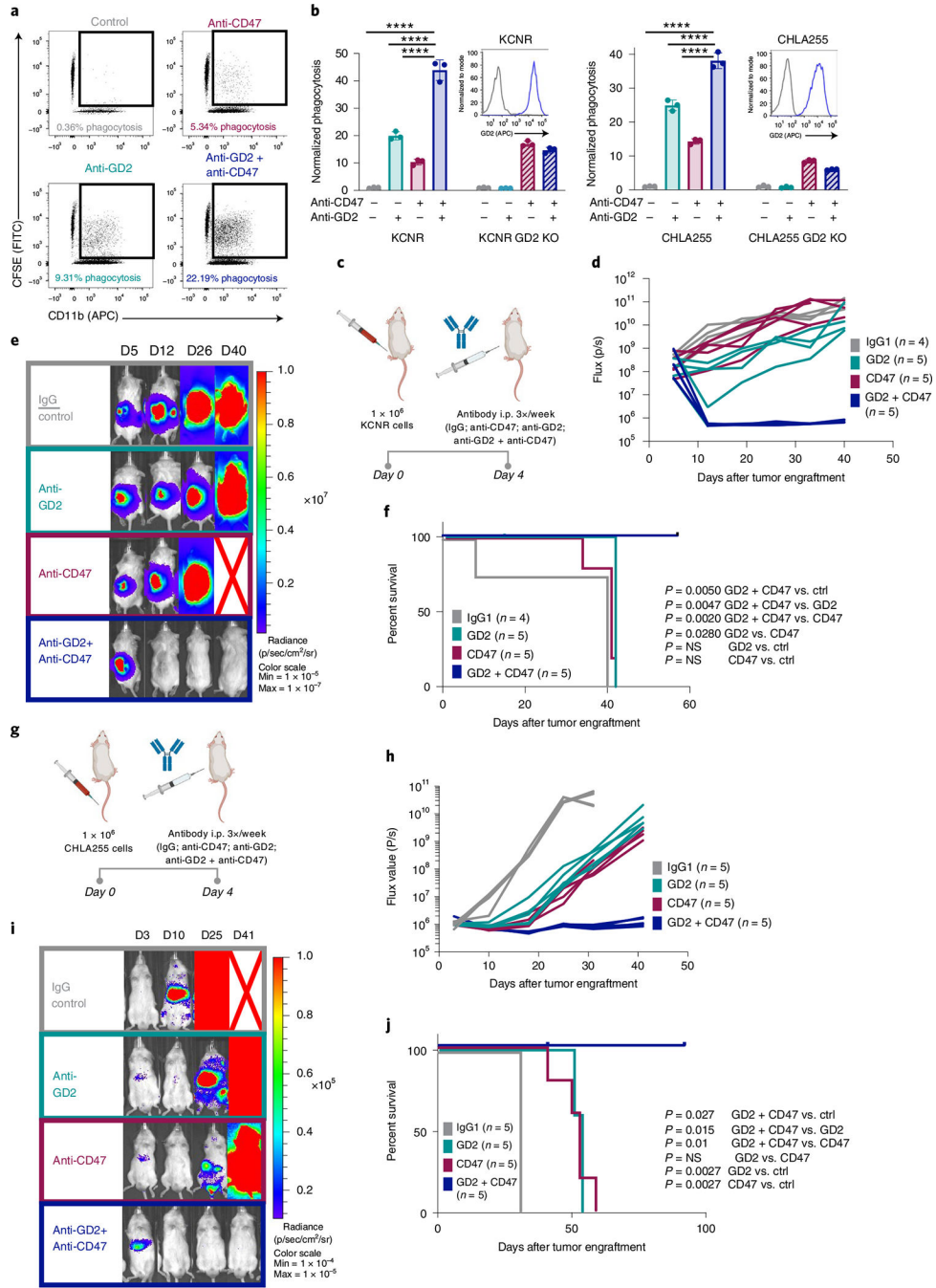
Fig. 1 |. Anti-CD47 and anti-GD2 synergize to mediate anti-tumor activity in xenograft models of neuroblastoma.

a, Representative flow cytometry plots depicting the phagocytosis of CFSE-labeled KCNR cells co-cultured with human-blood-derived macrophages in the presence or absence of anti-GD2 mAb, anti-CD47 mAb or dual treatment. **b**, Graphs show flow-cytometry-based quantification of phagocytosis of neuroblastoma cell lines in the presence of anti-GD2 mAb, anti-CD47 mAb or dual treatment, compared to untreated control; results normalized to the phagocytosis in the untreated control for each cell line and blood donor. Shown are mean ±

s.d. of three experimental replicates. Statistical comparisons were performed with one-way ANOVA with multiple comparison correction, ****$P < 0.0001$. KCNR: control versus anti-GD2 and anti-CD47, $P = 2.4 \times 10^{-14}$, anti-GD2 versus anti-GD2 and anti-CD47, $P = 5.7452 \times 10^{-11}$, anti-CD47 versus anti-GD2 and anti-CD47, $P = 3.66 \times 10^{-13}$; CHLA255: control versus anti-GD2 and anti-CD47, $P = 1.8 \times 10^{-14}$, anti-GD2 versus anti-GD2 and anti-CD47, $P = 1.43 \times 10^{-13}$, anti-CD47 versus anti-GD2 and anti-CD47, $P = 1.8 \times 10^{-14}$. Inset: flow histograms show surface GD2 expression on neuroblastoma cell lines used for each assay, blue: wild-type line, gray: GD2 KO (*B4GALNT1* KO) line. **a**, **b**, Representative data from at least three experiments performed with three different blood donors. **c**, Experimental overview of the orthotopic neuroblastoma model. **d**, Quantification of tumor progression for each individual mouse as measured by flux values acquired via BLI photometry. **e**, BLI images of representative mice from each treatment group shown in **d** at different time points. Red cross indicates deceased mouse. **f**, Survival curves for mice bearing tumors shown in **d**. Survival curves were compared using the log-rank test (two-tailed). **d–f** are representative of two independent experiments. $n = 5$ (anti-GD2 mAb, anti-CD47 mAb, anti-GD2/anti-CD47) and $n = 4$ (IgG control) mice per experiment. **g**, Experimental overview of the metastatic neuroblastoma model. **h**, Quantification of tumor progression for each individual mouse as measured by flux values acquired via BLI photometry. **i**, BLI images of representative mice from each treatment group shown in **h** at different time points. Red cross indicates deceased mouse. **j**, Survival curves for mice bearing tumors shown in **h**. Survival curves were compared using the log-rank test (two-tailed). **h–j** are representative of four independent experiments. $n = 5$ per group in each experiment. APC, allophycocyanin; FITC, fluorescein isothiocyanate; i.p., intraperitoneally; mAb, monoclonal antibody.
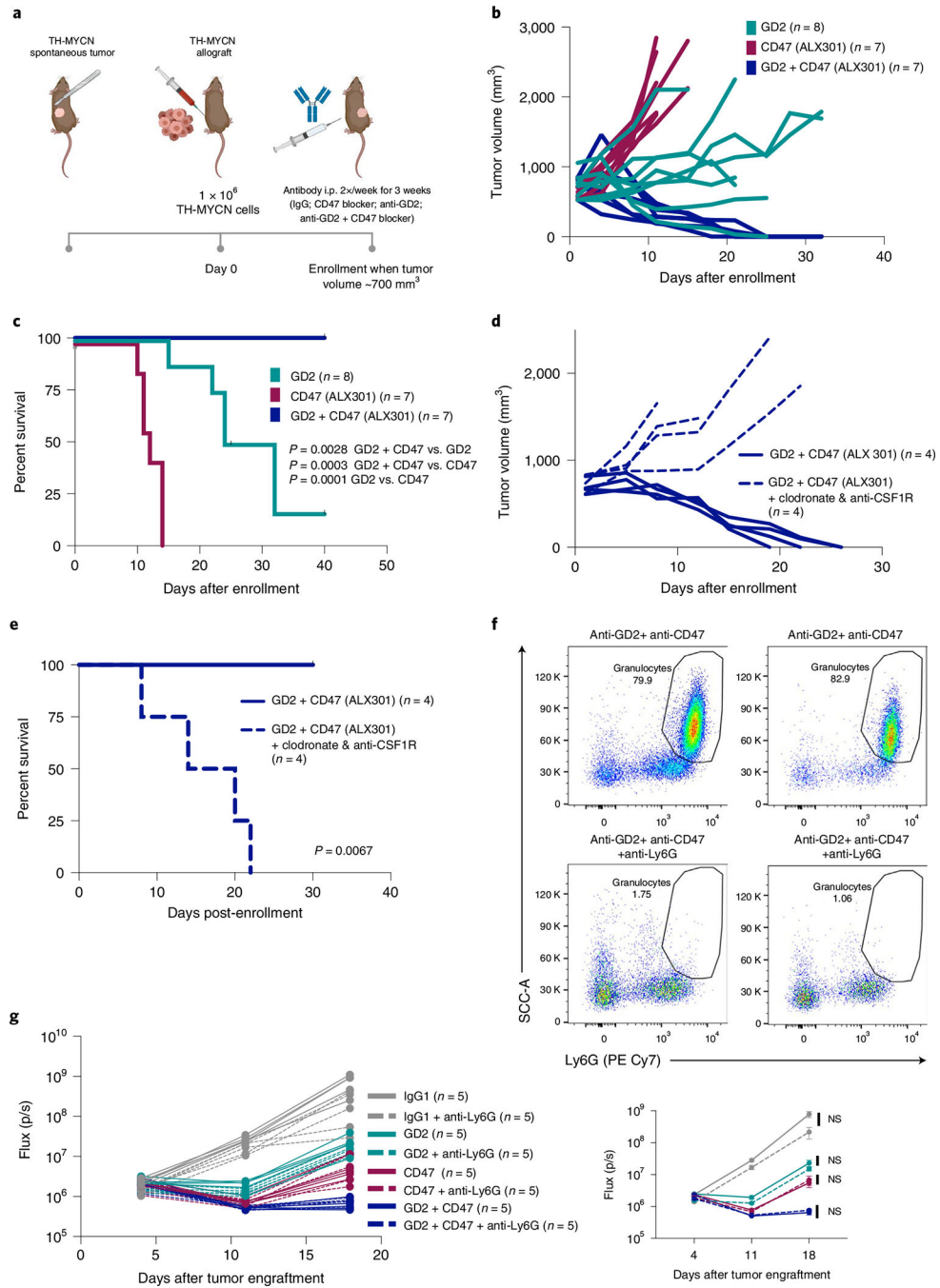
Fig. 2 |. CD47 blockade licenses TAMs to enhance the activity of anti-GD2 in a syngeneic model of neuroblastoma.

a, Experimental overview of the syngeneic model of neuroblastoma. One million cells from de novo tumors from TH-MYCN mice were harvested and injected subcutaneously into the flank of 129X1/SvJ mice. Once tumors reached a volume of ~700 mm^3, mice were injected with anti-GD2 mAb (14G2a), CD47 blocker (ALX301) or dual anti-GD2/CD47 blocker treatment twice a week for 3 weeks. **b**, Tumor progression for each individual mouse was followed using caliper measurements of tumor dimensions. **c**, Survival curves for mice

bearing tumors shown in **b**. Survival curves were compared using the log-rank test (two-tailed). Data for **a–c** are are from two pooled experiments with $n = 7$ (anti-CD47, anti-GD2/anti-CD47) and $n = 8$ (anti-GD2) mice per group. **d**, Mice received clodronate liposomes and anti-CSF1R mAb or no depletion alongside anti-GD2/CD47 blocker. Tumor progression for each individual mouse was followed using caliper measurements of tumor dimensions. **e**, Survival curves for mice from **d**. Survival curves were compared using the log-rank test (two-tailed). $n = 4$ mice per group. **f, g**, Mice treated with anti-Ly6G mAb were enrolled into the metastatic model of neuroblastoma as in Fig. 1g. **f**, Flow cytometry showing depletion of granulocytes in blood samples from mice treated with anti-Ly6G (bottom) versus control mice (top). **g**, Quantification of tumor progression for each individual mouse (left) as well as mean ± s.e.m. per treatment group (right) as measured by flux values acquired via BLI photometry. Statistical comparisons were made between Ly6G depleted and non-depleted groups using repeated-measures two-way ANOVA (NS denotes not significant, $P > 0.05$). The experiment was performed one time with $n = 5$ mice per group. i.p., intraperitoneally; mAb, monoclonal antibody.
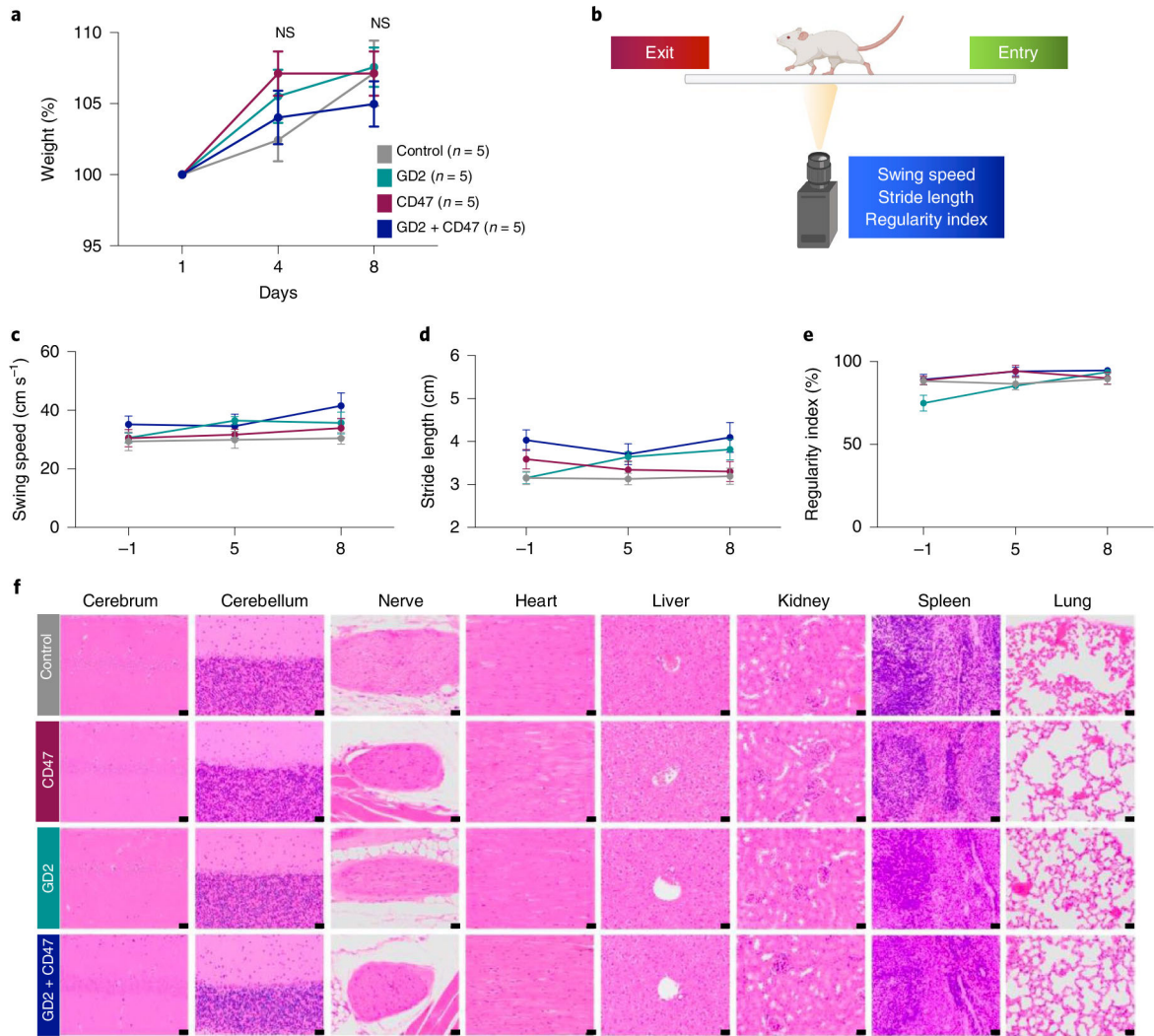
Fig. 3 |. Absence of neurotoxicity related to combined anti-GD2 and anti-CD47 treatment.
a, Non-tumor-bearing 129X1/SvJ mice were treated with anti-GD2 (14G2a), CD47 blocker (ALX301) or the combination of anti-GD2 (14G2a) and CD47 blocker (ALX301) for a total of three doses, and percent weight change during antibody treatment was recorded. Data shown are mean ± s.e.m. **b–e**, Mice performed CatWalk gait analysis at indicated time points, and swing speed (**c**), stride length (**d**) and regularity index (**e**) were measured. Data shown are mean ± s.e.m. **f**, H&E-stained sections of all examined organs were within normal limits as assessed by bright-field microscopy. Shown are sections of cerebrum, cerebellum, peripheral nerve, heart, liver, kidney, spleen and lung of animals from different experimental groups: (1) control, (2) CD47 blocker (ALX301) treatment, (3) anti-GD2 (14G2a) antibody treatment and (4) combined CD47 blocker (ALX301)/anti-GD2 (14G2a) antibody treatment. Magnification: ×40; scale bars, 20 μm. **a–f**, The experiment was performed once with $n = 5$ mice per group.
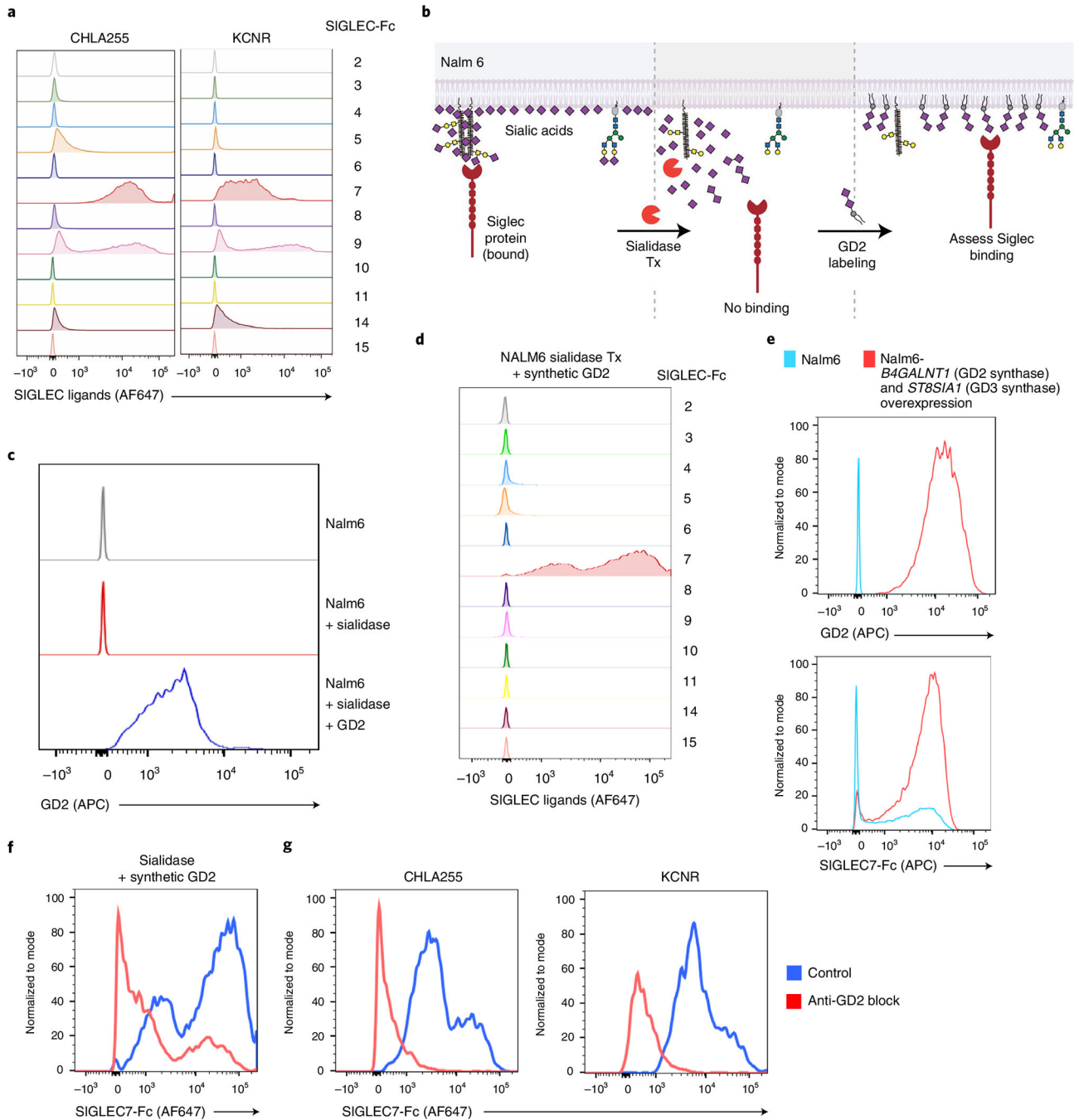
Fig. 4 |. Anti-GD2 blocks the interaction of GD2 with its ligand Siglec-7, an inhibitory immune receptor.

a, Flow cytometric histograms of CHLA255 and KCNR stained with recombinant human Siglecs. **b**, Experimental overview for the analysis of Siglec binding specificity to sialic-acid-stripped and GD2-coated Nalm6 cells. **c**, Flow cytometric histograms showing intensity of GD2 staining of Nalm6 cells (top), Nalm6 cells treated with sialidases (middle) and Nalm6 cells treated with sialidases and coated with GD2 (bottom). **d**, Flow cytometric histograms showing staining of Nalm6 cells pre-treated with sialidase and coated with

GD2 as in **b** with each individual recombinant Siglec. **e**, Flow cytometric analysis of the expression of GD2 (top) and Siglec-7 ligands (bottom) on the surface of wild-type Nalm6 cells or Nalm6 cells transduced with lentiviral constructs expressing *B4GALNT1* (GD2 synthase) and *ST8SIA1* (GD3 synthase). **f**, Flow cytometric analysis of Siglec-7 binding to Nalm6 treated as in **b** before (control, blue) and after (red) incubation with anti-GD2 mAb. **g**, Flow cytometric analysis of Siglec-7 binding to neuroblastoma cell lines CHLA255 and KCNR before (control, blue) and after (red) incubation with anti-GD2 mAb. APC, allophycocyanin; mAb, monoclonal antibody.
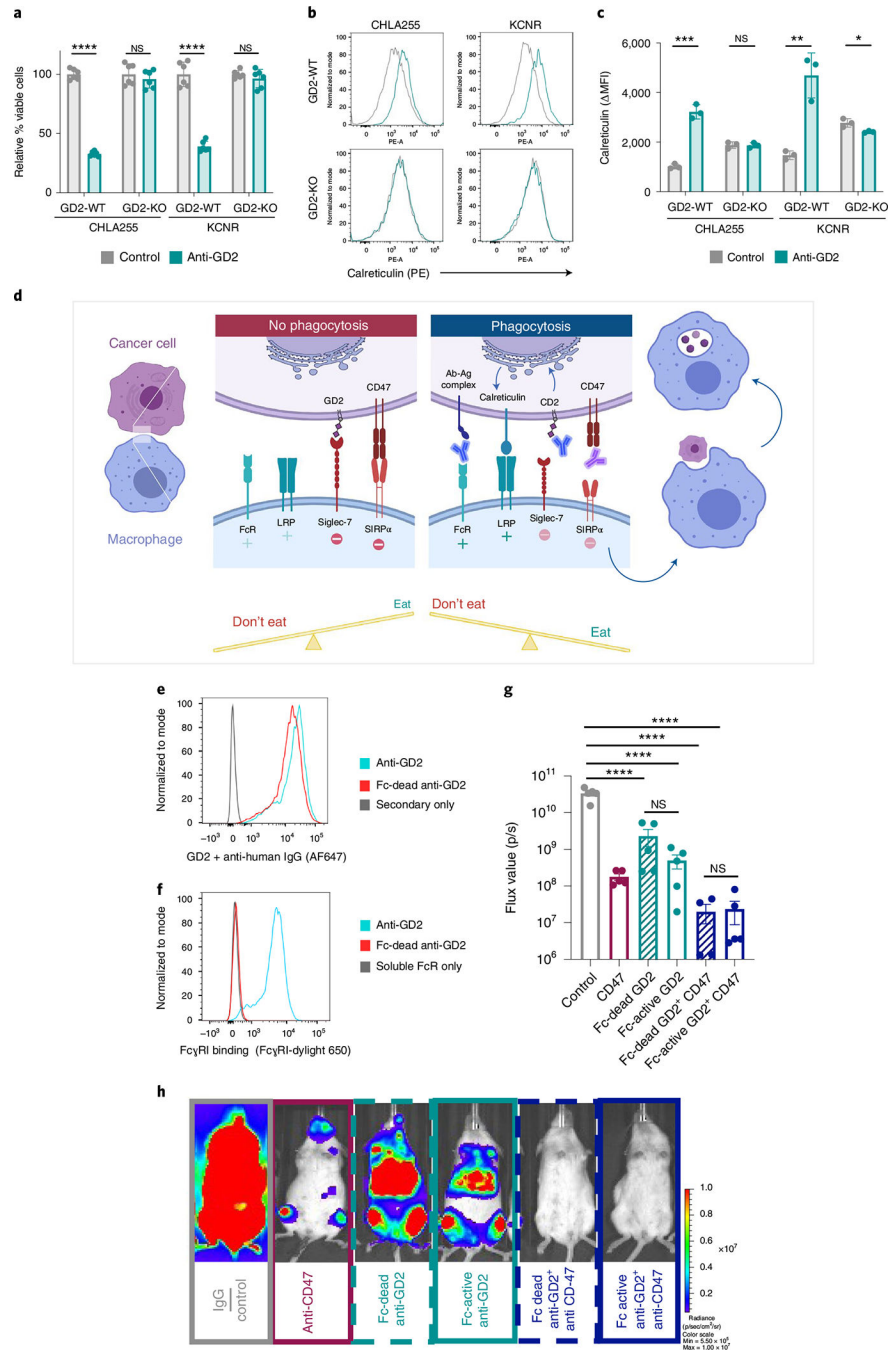
Fig. 5 |. Anti-GD2 antibody primes neuroblastoma cells for removal by the immune system.
a, Graph shows flow-based quantification of cell viability after incubation with anti-GD2 for 12 h normalized to the untreated control. Data shown are the mean ± s.d. of six experimental replicates. Statistical comparisons were performed with the unpaired *t*-test. CHLA255 $P = 1.2983 \times 10^{-11}$, CHLA255-GD2KO $P = 0.4125$, KCNR $P = 1.1405 \times 10^{-7}$, KCNR-GD2 KO $P = 0.3223$. **b**, Representative histograms of the expression of calreticulin on the surface of neuroblastoma cells after incubation with anti-GD2. **c**, Graph shows quantification of the expression of calreticulin (MFI) on the surface of neuroblastoma cell lines treated as in

a. Data shown are the mean ± s.d. of three experimental replicates. Statistical comparisons were performed with the unpaired *t*-test. CHLA255 *P* = 0.0002, CHLA255-GD2KO *P* = 0.9024, KCNR *P* = 0.0038, KCNR-GD2 KO *P* = 0.023. **a**–**c** were performed three times. **d**, Proposed model of synergy of anti-GD2 and anti-CD47. At baseline, tumor cells express CD47 and GD2, which bind to SIRPα and Siglec-7, respectively, on the surface of the macrophage, both of which are 'Don't eat me' signals that inhibit phagocytosis. Anti-GD2 blocks GD2:Siglec-7 interactions and induces export of calreticulin to the cell surface, upregulating an 'Eat me' signal. In the presence of anti-CD47, the balance of macrophage activity is shifted toward phagocytosis. **e**, Flow cytometric analysis of anti-GD2 and Fc-dead anti-GD2 mAb binding to GD2 on CHLA255 cells. Both antibodies were detected with a fluorophore-labeled secondary donkey anti-human IgG antibody. **f**, Flow cytometric detection of anti-GD2, but not Fc-dead anti-GD2, bound to CHLA255 cells detected with recombinant FcγRI-Dylight650. **g**, **h**, Metastatic neuroblastoma model as described in Fig. 1g. **g**, Quantification of tumor burden for individual mice on day 24 as measured by flux values acquired via BLI photometry. **h**, BLI images of representative mice from each treatment group shown in **g**. The experiment was performed one time. Data shown are mean ± s.e.m for *n* = 5 mice per group. Statistical comparisons performed with one-way ANOVA with multiple comparison correction. Fc-dead-GD2 versus control *P* = 1.52509×10^{-8}, control versus Fc-active-GD2 *P* = 5.20468×10^{-9}, Fc-dead-GD2 + CD47 versus control *P* = 1.20949×10^{-8}, control versus Fc-active-GD2 + CD47 *P* = 3.96719×10^{-9}, Fc-dead-GD2 versus Fc-active-GD2 *P* = 0.992 and Fc-dead-GD2 + CD47 versus Fc-active-GD2 + CD47 *P* > 0.999. *P < 0.05, **P < 0.01, ***P < 0.001, ****P < 0.0001 and NS P > 0.05. mAb, monoclonal antibody; NS, not significant.
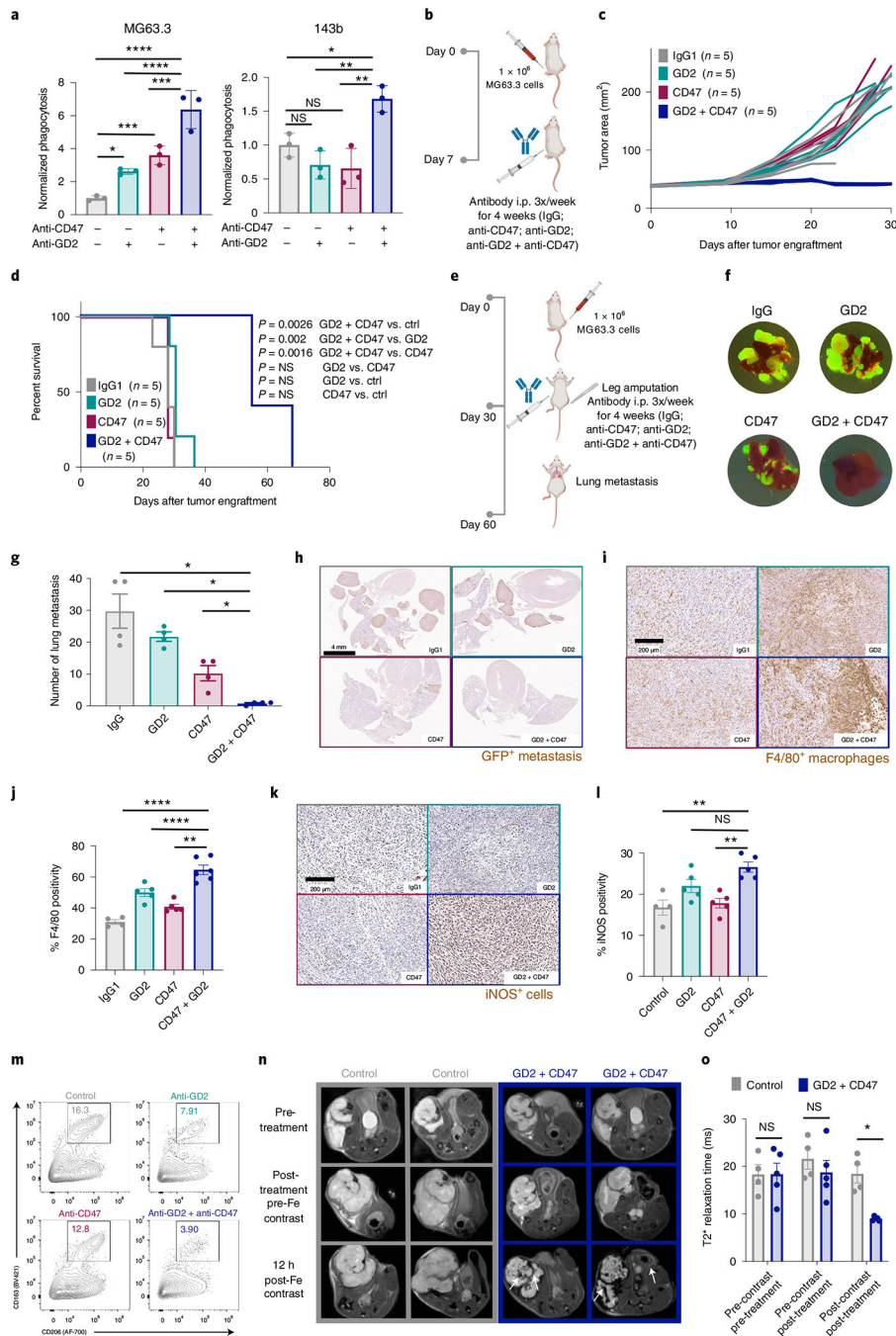
Fig. 6 |. Anti-CD47 and anti-GD2 elicit anti-tumor responses in models of osteosarcoma via TAM activation.

a, Quantification of phagocytosis of osteosarcoma cell normalized to phagocytosis in the untreated control. Data shown are mean ± s.d. of three experimental replicates. Statistical comparisons were performed with one-way-ANOVA with multiple comparison correction. MG63.3: control versus anti-GD2 $P = 0.0283$, control versus anti-CD47 $P = 0.0007$, control versus anti-GD2 and anti-CD47 $P = 4.6064 \times 10^{-7}$, anti-GD2 versus anti-GD2 and anti-CD47 $P = 2.20048 \times 10^{-5}$, anti-CD47 versus anti-GD2 and anti-CD47 $P = 0.0004$. 143b:

control versus anti-GD2 $P = 0.6849$, control versus anti-CD47 $P = 0.535$, control versus anti-GD2 and anti-CD47 $P = 0.0435$, anti-GD2 versus anti-GD2 and anti-CD47 $P = 0.0037$, anti-CD47 versus anti-GD2 and anti-CD47 $P = 0.0024$. Representative data from three experiments performed with three blood donors. **b**, Experimental overview of the orthotopic model of osteosarcoma. **c**, Tumor progression for mice treated as in **b**. **d**, Survival curves for mice shown in **c** compared by log-rank test (two-tailed). **b–d** are representative of three independent experiments with $n = 5$ mice per group. **e**, Experimental overview of metastatic model of osteosarcoma. **f**, Representative images of GFP$^+$ metastases in lungs from treated mice. **g**, Quantification of metastases from **f**. Data shown are mean ± s.e.m. of $n = 4$ biologic replicates. Statistical comparisons as in **a**. GD2 + CD47 versus CD47 $P = 0.0286$, GD2 + CD47 versus IgG $P = 0.0286$, GD2 + CD47 versus GD2 $P = 0.0286$. Representative of two independent experiments. **h**, Representative IHC images showing lung metastases. **i–o** Mice were treated with indicated antibodies for 7 d after tumors grew for 21 d. **i**, Representative IHC images showing detection of macrophages (anti-F4/80). **j**, Quantification of **i**. **k**, Representative IHC images showing staining with anti-iNOS. **l**, Quantification of **k**. **j**, **l**, Data are the mean ± s.e.m. of 4–5 biologic replicates. Statistical comparisons as in **a**. F4/80: IgG1 versus CD47 + GD2 $P = 2.6746 \times 10^{-7}$, CD47 versus CD47 + GD2 $P = 1.0476 \times 10^{-5}$, GD2 versus CD47 + GD2 $P = 0.0020$. iNOS: IgG1 versus CD47 + GD2 $P = 0.0016$, CD47 versus CD47 + GD2 $P = 0.0025$, GD2 versus CD47 + GD2 $P = 0.1399$. **m**, Representative flow plots of M2 macrophages (CD163$^+$/CD206$^+$). **n**, Representative magnetic resonance images of mouse tumors pre-treatment and post-treatment, before or 12 h after ferumoxytol. Arrows point to hypointense areas of iron-labeled macrophages. **o**, Quantification of T2* relaxation time from **n**. Data shown are mean ± s.e.m. of four biologic replicates. Statistical comparisons were made between groups with the Mann–Whitney test (unpaired, two-sided). Pre-contrast/pre-treatment $P > 0.9999$, pre-contrast/post-treatment $P = 0.4127$, post-contrast/post-treatment $P = 0.0159$. *$P < 0.05$, **$P < 0.01$, ***$P < 0.001$, ****$P < 0.0001$ and NS $P > 0.05$. i.p., intraperitoneally; NS, not significant.